PHYSICAL CHARACTERIZATION OF THE RACK EFFECT AND HYDROGEN BOND NETWORKS IN BLUE COPPER PROTEINS

Thesis by

Michael C. Machczynski

In Partial Fulfillment of the Requirements

For the Degree of

Doctor of Philosophy

California Institute of Technology

Pasadena, California

2001

(Defended August 17, 2000)

© 2001

Michael C. Machczynski

All Rights Reserved

Abstract:

A summary of previous research is presented that indicates that the purpose of a blue copper protein's fold and hydrogen bond network, aka, the rack effect, enforce a copper(II) geometry around the copper(I) ion in the metal site. In several blue copper proteins, the C-terminal histidine ligand becomes protonated and detaches from the copper in the reduced forms. Mutants of amicyanin from *Paracoccus denitrificans* were made to alter the hydrogen bond network and quantify the rack effect by pK_a shifts.

The pK_a's of mutant amicyanins have been measured by pH-dependent electrochemistry. P94F and P94A mutations loosen the Northern loop, allowing the reduced copper to adopt a relaxed conformation: the ability to relax drives the reduction potentials up. The measured potentials are 265 (wild type), 380 (P94A), and 415 (P94F) mV vs. NHE. The measured pK_a's are 7.0 (wild type), 6.3 (P94A), and 5.0 (P94F). The additional hydrogen bond to the thiolate in the mutants is indicated by a red-shift in the blue copper absorption and an increase in the parallel hyperfine splitting in the EPR spectrum. This hydrogen bond is invoked as the cause for the increased stability of the C-terminal imidazole.

Melting curves give a measure of the thermal stability of the protein. A thermodynamic intermediate with pH-dependent reversibility is revealed. Comparisons with the electrochemistry and apoamicyanin suggest that the intermediate involves the region of the protein near the metal site. This region is destabilized in the P94F mutant; coupled with the evidence that the imidazole is stabilized under the same conditions confirms an original concept of the rack effect: a high energy configuration is stabilized at a cost to the rest of the protein.

Chapter 1:

Blue Copper Proteins and the Rack Effect

Introduction to Electron Transfer:

Electron transfer reactions occur widely in chemistry and biology[1,2]. Storage and rapid movement of electrons are necessary to effect nearly every chemical reaction. If electron transfer is fast, then it may be readily triggered by complex systems such as protein-protein and protein-small molecule binding that allow greater finesse and control in the cellular environment. The ground rules for facile electron transfer have been revealed through many years of work and may be represented by the semiclassical expression[3]:

$$k_{ET} = \frac{2\pi^2}{h\sqrt{\pi\lambda kT}} H_{AB}^2 \exp\left(-\frac{\left(\Delta G^0 + \lambda\right)^2}{4\lambda kT}\right)$$

Here, ΔG^0 is the standard free energy of the reaction, λ is the reorganization energy required for electron transfer, and H_{AB} is the electronic coupling matrix element. When the energy levels of the electron donor and acceptor are distant from the energy levels of the intervening medium, as is the case in proteins, electron transfer occurs through a superexchange mechanism[4] and H_{AB} decays exponentially with distance, r (where r_0 is the distance when the orbitals are in direct contact):

$$H_{AB}^2 = H_0^2 \exp(-\beta(r - r_0))$$

The superexchange mechanism is often visualized as the orbitals of the electron donor coupling through the σ-bond framework of the intervening medium[3]. Thus, H_{AB} is also

called the electronic factor of the semiclassical electron transfer expression. It is clear that one way nature can maximize the rate for electron transfer is to minimize the distance between the donor and acceptor.

The rest of the semiclassical expression is known as the nuclear factor because the relationship between ΔG^0 and λ determines what the position of the nuclei must be for the transition state to be reached. The exponential term within the nuclear factor was a source of controversy for many years; it predicts that the rate of electron transfer actually decreases with increasing driving force once a maximum (where $\Delta G^0=\lambda$) is reached. Experimental evidence has shown that this so-called "inverted" region exists[5]. For rapid electron transfer, it is desirable that ΔG^0 is as close to λ as possible. Biological electron transfer usually requires many steps before reaching the electron's final destination. Since the electrochemical potential involved is limited by the oxidation/reduction of water, the total potential change is less than 1.6 eV. Dividing the potential between several electron transfer steps shows that the driving force for a biological electron transfer reaction can only be a few hundred millivolts at most. This number is small, so nature must minimize the reorganization energy to achieve rapid electron transfer. The reorganization energy has two terms associated with it: the inner-sphere term is small when there are few bonding rearrangements at the redox center, while the outer-sphere term is small when solvent molecules are sequestered from the site. The exclusion of solvent molecules essentially reduces the amount of change that occurs when an electron is added or removed from the metal because the solvent has a much higher dielectric constant than the protein.

Nature harnesses copper's potent redox abilities in order to store electrons in a chemically useful manner, as well as to perform chemistry directly[6]. The type one site exists solely for the purposes of electron storage and transport. The type one site became of interest early due to its intense blue color ($\varepsilon \sim 2000\text{-}6000\ M^{-1}\ cm^{-1}$ near 600 nm), small hyperfine splitting ($A_{\|}$ 50-90 x $10^{-4}\ cm^{-1}$), and high reduction potentials (originally 300-500 mV vs. NHE, compared to aqueous copper at 150 mV). Structurally, these sites are distinguished by trigonal planar coordination of the copper by two histidines and a cysteine, and usually possess a long (2.8-3.5 angstrom) bond to a methionine thioether in the axial position. In azurin, a carbonyl oxygen interacts with the copper at an axial position opposite to the methionine. The highly covalent bond to the cysteine is responsible for its surprising spectroscopy[7]. Many bacteria and plants contain small (10-20 kDa) proteins that seem to possess a blue copper site as their only prominent feature. These proteins are mostly beta sheet in structure. Examples of these proteins, to which comparisons in this thesis are made, include azurin, plastocyanin, amicyanin, rusticyanin, umecyanin, and stellacyanin. The type one site has a low reorganization energy that makes it ideal for the giving and receiving of electrons. It is thus also used as a storage battery in larger proteins that need to have an electron (or hole) available for chemistry. The rack effect is a theory that attempts to explain how low reorganization energy is achieved by the type one site.

Current status of the rack:

As stated above, blue copper proteins are small (10-20 kDa) electron transferases with conserved His_2Cys residues that bind copper in a prearranged trigonal site, typically with a long axial bond (2.5 - 3.2 Å) to a methionine thioether[8] (Figure 1.1). To achieve facile electron transfer within biological systems, reorganization of the redox center upon reduction/oxidation must be minimized[9]. Cupric ions are known to favor tetragonal structures, while cuprous ions are commonly found in trigonal or tetrahedral arrangements (Table 1.1).[6] These arguments led Malmström to propose that the cupredoxin fold is a "rack" that forces copper(II) into the copper(I) geometry, restricting the conformational changes associated with the redox process[10]. The reorganization energy of azurin is 0.8 eV[11,12], while that of the unfolded azurin is estimated to be ~2.4 eV[9]. These numbers suggest that the cupredoxin fold is responsible for enhancing the rate of the self-exchange reaction by a factor of $\sim 5 \times 10^7$.

Table 1.1: Copper coordination in inorganic compounds.

Coordination Number	Core (additional donor atoms)	Geometry	Cambridge Structural Database System Codes[1] (additional donor atoms)
6	$Cu(II)N_2S(XYZ)$	Square bipyramidal	COGNAN01(SSS); HAZKAU(OOO); JETMIE(SNN); JUXTIF(SNN); PANPID(SOO); PEWWET(SClCl); PEWWIX(SClCl); PITUCU(SOO); SEYNOZ(SNN)(3);[2] VUWGUP(SNN); VUWHAW(SNN)(2);[2] CIYNAZ(OOO); FICVIW(NNS); NAHDEF(SNN); PIATCU(SOO); RACMAJ(SOO)(2);[2] SOFXUG(OOO)
5	$Cu(II)N_2S(XY)$	Square pyramidal	BPYTCU(NN); BULTUX(NN); COHHIQ(NN); JECXEU(NN); ROQDEG(ON)(1);[2] TIVTAT(NO); TPAECU(OO); ZEDNIF(OO); FENMEQ(OO); FENMIU(OO); FIPFOZ(OO)(2);[2] GERPAU(OO); GLXZCU(ClCl); KEXVAC(ON); KEXVEO(NN); KUTSOH(SO)(4);[2] LESTIM(ClCl); LEYXUI(SCl); RIHMOK(NO); RONBOL(OO)(2);[2] SAHDOU(NN); SODZIU(NN); SOFXDA(OO); TIMQEL(SCl);

			TOQFAG(BrBr); VOBSAG(OO); ZEBLIB(ClCl)
		Trigonal bipyramidal	MAECUT(OO); PLTUCU(NN); RUQLOE(NO); TIVTEX(NO); KUCZEN(NO); LEYYAP(BrS); NEGWUR(OO); NIVDAX(NN); RUTBAJ(NN); RUTBEN(NN); ZAMCUL(NN)

4	$Cu(II)N_2S(X)$	Square planar	COGMUG(S); CXTPAC(S); LESBAM(S); MEQUCU10(S); NAQPAW(N); QQQDSX02(S); CONBUC(O); FIPFOZ(O)(2);[2] HEDSAK(Br); NEGXAY(O); NIJXOT(Br); VEPFAX10(O); VEPFEB10(O); WEWSAS(Br); YUNRII(Br); ZEBLEX(Cl); ZOWRAE(O)
		Tetrahedral	CIWVIN(S); FONXIP(S); SOFXOA(O); PANDAJ(N); TMCTCU(S)
	$Cu(I)N_2S(X)$	Tetrahedral	BUYBAY(S); CEWYOS10(S); CUHBAI(N); CUHBOW(N)(2);[2] CUHBUC(N); DIYKOL(S); GIKDUZ(P); HEFJIL(S)(1);[2] JADDUN(S); NIRJED(P)(1);[2] PBTUCU(S); PYDSCU10(N); RISWEV(S);[2] SISFEF(S); SISFIJ(S); TOYBOY(S)(1);[2] YINJIO(S); NBTPCU(N)
3	$Cu(I)N_2S$	Trigonal planar	CUGZUZ; HICVIY; JONZOB; NILBEP; NILBIT; PAFZUR; VETFEF; YOMJOZ(1);[2] YOMJUF(1);[2] BETYUU

[1]Codes as listed in January, 1999. [2]In structures with more than one copper atom in the asymmetric unit, the number of structures with the given geometry is listed in parentheses.

The first question raised by this structural hypothesis is: does the type 1 (T1) copper site force the ligands into a prearranged metal binding structure? Crystal structures of the apo-forms of plastocyanin[13] and azurin[14,15] reveal structures nearly identical with those of the holo-forms. However, it has been shown that in plastocyanin, removal of copper causes significant changes in the CD spectrum[16], suggesting that packing forces or the high salt concentrations of crystallographic buffers[17] may cause the crystal structure to differ significantly from the solution structure. In the reduced forms of plastocyanin[17], amicyanin[18,19], and pseudoazurin[20], the C-terminal histidine ligand protonates, detaches

from the metal, and rotates around its C^{β}-C^{γ} bond to assume a position identical with that found in the apoprotein (Figure1.2); this reduction in coordination number causes shortening of the copper methionine bond (2.9 to 2.5 Å) that results in a trigonal Met-His-Cys species. In the H117G mutant of azurin, a cavity is formed that allows exogenous ligands to bind[21]. Imidazole binds the copper(II) form but is ejected from the cavity upon copper reduction. Ryde *et al.* predict that the imidazole is removed from copper as they use better basis sets in their calculations[22]. These observations suggest that the C-terminal imidazole must be forced to the copper. Examining the large number of crystal structures solved for native blue copper proteins reveals that the histidine and cysteine bond angles and lengths (Table 1.2)[6] are highly similar between species. The area near these equatorial residues is highly structured due to a large number of long-range (in sequence space) hydrogen bonds (Figure 1.3). Eleven of the sixteen long-range hydrogen bonds in the azurin from *Alcaligenes denitrificans* are found in this region, also known as the northern loop[23].

Table 1.2: Metal-ligand bond distances (Å).

P. aeruginosa azurin	M-N^{δ}1 (His46)	M-S^{γ} (Cys112)	M-N^{δ}1 (His117)	M-S^{δ} (Met121)	M-O (Gly45)	PDB code [ref]
Cu(II) (pH 5.5)[1]	2.08	2.24	2.01	3.15	2.97	4AZU [24]
Cu(I) (pH 5.5)[1]	2.14	2.25	2.04	2.97	3.15	N/A [25]
Cu(II) (pH 9.0)[1]	2.06	2.26	2.03	3.13	2.93	5AZU [24]
Cu(I) (pH 9.0)[1]	2.14	2.27	2.15	3.10	3.17	N/A [25]
Co(II)[1]	2.32	2.20	2.25	3.49	2.15	1VLX [26]
Ni(II)[1]	2.23	2.39	2.22	3.30	2.46	N/A [27]

Zn(II)[1,3]	2.01	2.30	2.07	3.4	2.32	N/A [28]
A. denitrificans azurin						
Cu(II)	2.08	2.15	2.00	3.11	3.13	2AZA [29]
Cu(I)	2.13	2.26	2.05	3.23	3.22	N/A [30]
Cd(II)	2.25	2.38	2.21	3.23	2.76	1AIZ [31]
P. nigra plastocyanin	M-N$^{\delta 1}$ (His37)	M-S$^{\gamma}$ (Cys84)	M-N$^{\delta 1}$ (His87)	M-S$^{\delta}$ (Met92)		
Cu(II) (pH 6.0)	1.91	2.07	2.06	2.82		1PLC [32]
Cu(I) (pH 7.0)	2.13	2.17	2.39	2.87		5PCY [32]
Cu(I) (pH 7.8)[3]	2.12	2.11	2.25	2.90		4PCY [33]
Hg(II)	2.34	2.38	2.36	3.02		3PCY [34]
S. sp. PCC 7942 plastocyanin						
Cu(II) (pH 5.0)	1.97	2.01	2.14	2.93		1BXU[35]
Cu(I) (pH 5.0)	2.09	2.37	2.17	2.80		1BXV[35]
D. crassirhizoma plastocyanin	M-N$^{\delta 1}$ (His37)	M-S$^{\gamma}$ (Cys87)	M-N$^{\delta 1}$ (His90)	M-S$^{\delta}$ (Met95)		
Cu(II) (pH 4.5)	1.99	2.23	2.06	2.94		1KDJ [36]
Cu(I) (pH 4.5)	1.95	2.21	2.10	2.91		1KDI [36]
A. faecalis S-6 pseudoazurin	M-N$^{\delta 1}$ (His40)	M-S$^{\gamma}$ (Cys78)	M-N$^{\delta 1}$ (His81)	M-S$^{\delta}$ (Met86)		
Cu(II) (pH 6.8)	2.16	2.16	2.12	2.76		1PAZ [37]
Cu(I) (pH 7.8)	2.16	2.17	2.29	2.91		1PZA [38]
Cu(II)	2.01	2.13	2.01	2.71		8PAZ[39]
Cu(I) (pH 7.0)	2.10	2.17	2.31	2.82		3PAZ[39]

A. cycloclastes pseudoazurin					
Cu(II) (pH 6.0)	1.95	2.13	1.92	2.71	1BQK [40]
Cu(I) (pH 6.0)	2.04	2.19	2.11	2.85	1BQR [40]
T. ferrooxidans rusticyanin	M-N$^{\delta 1}$ (His85)	M-S$^{\gamma}$ (Cys138)	M-N$^{\delta 1}$ (His143)	M-S$^{\delta}$ (Met148)	
Cu(II) (pH 4.6)	2.04	2.26	1.89	2.89	1RCY [41]
Cu(I)	2.22	2.25	1.95	2.75	1A3Z [41]
Cu(I)[3]	2.14	2.26	2.06	2.90	1A8Z [42]
Cu(I) (pH 3.4)[4]	2.09	2.16	1.90	2.60	1CUR [43]
Ascorbate oxidase	M-N$^{\delta 1}$ (His445)	M-S$^{\gamma}$ (Cys507)	M-N$^{\delta 1}$ (His512)	M-S$^{\delta}$ (Met517)	
Cu(II) (pH 5.5)[1]	2.11	2.08	2.08	2.86	1AOZ [44]
Cu(I)[1,3]	2.12	2.14	2.08	2.95	1ASO [45]

[1]Average metal-ligand bond distances are reported in cases where there are multiple molecules in the crystallographic asymmetric unit. [2]Atomic coordinates have not been deposited with the Protein Data Bank, Brookhaven National Laboratory. [3]Resolution lower than 2 Å. [4]NMR solution structure.

Mutations of the hydrogen bonds in this region often lead to dramatic changes in protein characteristics. Asp47 (in azurins), which immediately follows the N-terminal His ligand, is highly conserved[8]. The backbone amide forms a hydrogen bond with the thiolate of the cysteine ligand, while the sidechain nitrogen and amide each form a bond with the first Ser/Thr residue in the northern loop (Figure 1.4). Altering these hydrogen bonds frequently leads to an increased reduction potential[46] or copper loss[47]. Removal of the two bonds to the Ser/Thr residue also lowers the denaturation temperature by ten degrees.

The interpretation of these results is that the network functions as a clasp between the northern loop and the rest of the protein. The removal of these bonds loosens the structure of the active site. The trigonal plane is present in a rigid, prearranged form.

The axial ligand, however, takes up a variety of positions relative to the trigonal plane. There is an inverse correlation between the Cu-S(Met) and Cu-S(Cys) bond distances. The "softness" of the Cu-S(Cys) bond results in very small changes in bond length[48]. Originally, the large splitting in ligand field energies had been attributed to backbonding to the methionine ligand from the Cu $d_{xz,yz}$ orbitals[49]. PES studies have since shown that no backbonding occurs from the copper to the thioether, and that the sulfur acts solely as a donor[50]. The relative intensity of the two visible LMCT bands assigned to Cu($d(x^2-y^2)$)<- S(Cys(p pseudo-σ)) and Cu($d(x^2-y^2)$)<- S(Cys($p\pi$)) transitions, as well as the rhombicity of the EPR spectra, are very sensitive to the angular position of the axial ligand and the planarity of the site[51,52]. These values vary greatly in a manner predicted from the crystal structures.

Solomon and coworkers have proposed that the Cu-S(Met) bond length is finely tuned by the protein[53]. Their measurements and calculations show that in the protein, methionine donates less to the copper than it would in equilibrium[50]. They attribute this to the protein restricting the movement of the thioether sidechain. The Met backbone has intraloop hydrogen bonds to the His carbonyl and the Cys amide[39], while the sidechain is almost always sandwiched between two hydrophobic residues[8,54]. However, in the case of strong axial ligation, like the Met121His azurin, the copper is dramatically pulled out

of plane[55] (Figure 1.5). At low pH, His121 detaches and there is a massive rearrangement in the copper-binding loop following the His117 ligand. Thus, strong metal-ligand or steric interactions overwhelm whatever stability the loop possesses. Canters' group has replaced the northern loop of *P. versutus* amicyanin with the equivalent loops from azurin, plastocyanin, pseudoazurin, and nitrite reductase[56]. While the energies of the visible absorption bands remain (confirming the retention of the trigonal structure), once again the shifts in their relative intensities clearly show that the site becomes more rhombic (the Met is pushed away from the axial position) with increased loop length (Table 1.3). The spectra for the proteins with azurin and pseudoazurin loops are temperature dependent, indicating flexibility.

Table 1.3: Absorbance ratios of the loop mutants of *P. versutus* amicyanin.

Protein:	Amicyanin	Ami-Pcy[a]	Ami-Azurin	Ami-Paz[a]
$A_{\sim 460}/A_{\sim 600}$	0.10	0.26	0.19	0.28

[a] Ami-Pcy and Ami-Paz refer to the plastocyanin and pseudoazurin loop mutants of amicyanin respectively.

Apo-azurin readily binds zinc(II), cobalt(II), and nickel(II). These metals have similar ionic radii, cobalt being the largest. The crystal structures of all of these forms have been solved and show significantly more tetrahedral character and a compression of the axial ligands towards the metal site (carbonyl oxygen-S^{δ}(Met) distance shrinks from 5.88Å (Co^{II}) to 5.44Å (Ni^{II}))[57] (Table 1.4). There also exists a striking change in the carbonyl oxygen-metal-S^{δ}(Met) angle.

Table 1.4: Metal-ligand bond lengths in various divalent metal derivatives of *P. aeruginosa* azurin.

Metal to ligand bond length (Å)	Co-Azurin	Ni-Azurin	Zn-Azurin	Cu-Azurin
M to 45 C=O	2.15	2.46	2.32	2.97
M to 46 $N^{\delta 1}$	2.32	2.23	2.07	2.11
M to 112 S^{γ}	2.20	2.39	2.30	2.25
M to 117 $N^{\delta 1}$	2.25	2.22	2.01	2.03
M to 121 S^{δ}	3.49	3.30	3.38	3.15
45 O to 121 S^{δ}	5.51	5.44	5.88	5.78
45 O-M-121 S^{δ} angle (degrees)	155	141	180	141

In fact, the bond lengths and angles for each metal are in accord with the averages found in many model compounds of the respective metals. In addition, the bond length changes upon reduction are commensurate with the change in radius for the copper ion[58]. These observations demonstrate two things: the restraining force for methionine is not as great as proposed and the metal-equatorial ligand bond lengths are not unusual.

These structures raise the question of whether the observed geometry is deleterious for copper. Recent calculations suggest that the blue copper site is unstrained for both copper(II) and copper(I)[59]. However, most of these compounds are made in solution, with no protection from solvent molecules or other potential reactants. If one

were to limit the exposure of the metal to additional ligands, by use of noncoordinating solvent and ligands with bulky substituents, complexes similar to the protein should be able to form. Kitajima and coworkers have shown that this is the case by using pyrazolylborate and pentafluorinated phenyl thiolates in methylene chloride. These complexes possess visible absorption and EPR spectra very similar to blue copper[60,61]. The bond lengths and angles found in the crystal structure also match those of the protein, including the short thiolate bond that has not been found in other compounds[62]. Tolman has also recently prepared a compound with blue copper spectroscopic properties. It is important to note that these compounds have only been prepared and characterized in the copper(II) state. No functional analogues have been made to date. All that can be said, then, is that copper (II) is comfortable in the confines of a type one site.

It has already been shown that the protein stabilizes the transition state for electron transfer. It has also been shown that the scaffold is needed to enforce full ligation upon the reduced copper and to tune the reduction potential into the functional range. Elimination of one or two constraining hydrogen bonds as mentioned above leads to dramatically increased reduction potentials. The potential increase is actually 60 mV greater than that observed for the M121L mutation[46]! This behavior is attributed to a loosening of the ligand loops, thereby allowing the reduced form to reach a fully relaxed configuration. Thus it is apparent that copper(I) is strained in the folded protein. The fact that Kitajima was unable to measure reduction potentials for his complexes indicates that there may be a large structural change upon reduction. One method to probe the stability of the metal-protein complex is by denaturation. In order to understand the

relative stabilities of the copper(II)/copper(I) proteins, work done on the apo-forms must first be reviewed.

When apo-azurin is chemically denatured by guanidine hydrochloride (GdnHCl), the process exhibits two clearly separate phases in the far-UV circular dichroism spectra[63]: one phase, attributed to the active site, has a titration midpoint of 1.66 M. The midpoint of the second phase occurs at 3.09 M. Assignment of the first phase is supported by the fact that it disappears upon addition of zinc or copper; this disappearance also indicates an increase in protein stability upon metal binding. Two separate arguments may be made for the lower stability of the apo-form: Either the presence of the metal ties the protein together, or the lack of the metal allows the denaturant increased access to the hydrogen bond networks of the protein, as evidenced by solvent presence in the active site of the apo-protein. Thermal and low pH denaturations[64] also demonstrate that apo-azurin is less stable than either holo-form.

Which is more stabilized, copper(II) or copper(I)? When azurin is unfolded by GdnHCl, the reduction potential is raised[65]; apparent confirmation that the reduced form is more stable when unfolded. Indeed, two state fits to the denaturation curves give midpoints of 2.6 M for copper(I) and 3.9 M for copper(II)[63]. EXAFS and XAS indicate that the coordination of the unfolded, reduced form is 1.5 - 1 N(O) and 1.5 - 2 S(Cl) ligands[66], which could be interpreted as the His-Cys-Met ligation revealed by the low-pH plastocyanin crystal structure[17]. Thermal experiments present a conflicting view, however. The reduced form of azurin unfolds at only 3 degrees below the oxidized

protein[64], but reduced plastocyanin unfolds at ten degrees higher than that oxidized species[16]. GdnHCl unfolding of copper(II) often results in reduction of the copper by the thiolate ligand, with subsequent unfolding of the less stable reduced species, while thermal unfolding of copper(II) does not lead to reduction, as an EPR signal consistent with 2N,2O coordination (type two copper) is observed in the unfolded form[67]. It is clear that the different methods of denaturation produce different states of the proteins. It may also be that plastocyanin and azurin unfold differently, especially since plastocyanin has several highly charged patches and azurin's charge is spread homogeneously, with opposite charges often coupled to each other, across the surface[23].

Perhaps an understanding of the energetics of the metal-protein complex may be gained by comparing electrostatic effects vs. the differences in stabilities of d^9 and d^{10} metals. The NMR spectrum of cadmium(II)-substituted pea plastocyanin has been interpreted in terms of a hydrogen bonding network that is much more similar to copper(II) than copper(I)[68], suggesting that electrostatics are quite important in stabilizing the structure of the active site. However, GdnHCl denatures zinc(II)-azurin at 2.75 M, or approximately the same value as copper(I)-azurin[63]. It is interesting that both the lower and higher Gdn unfolding phases of apo-azurin disappear when metallated, suggesting that the stability of the metal site is increased at a cost to the rest of the protein. This idea of sacrificing global energy to achieve local strain has been a core rack concept since its inception[69]. Copper(II)-azurin is far more stable than apo-azurin, reinforcing our statement earlier that the cupric ion is comfortable in a type one site. While the electronic environment of the hydrogen bonds may change based on

electrostatics, the unfolding curves are a better measure of protein stability, and so it is concluded that the stuctural preferences of d^9 and d^{10} ions rather than electrostatics control the structure of the metal site.

Finally, the previously mentioned case of thermally denatured azurin with its EPR signal corresponding to 2N, 2O coordination, raises another role of the protein fold: exclusion of solvent. The oxygen coordination in the unfolded structure is ascribed to water molecules, yet there is no sign of them in the folded protein. The various azurin ligand mutations H117G[21], H46G[70], and M121X (X = Gly, Ala, Val, or Leu)[71] all have external ligands binding in the cavities left by their mutations. Often, the ligand is water/hydroxide, but many other ions and small molecules may exhibit this behavior. This occurrence means that water is at most an imidazole away from the copper. The dissociation constants for the M121X mutants decrease with less sidechain packing from the 121 residue. Since the difficulty of electron transfer for the $Cu^{II/I}$ couple in solvent is known and these perturbations in the protein matrix all result in solvent penetration, it is apparent that another role of the protein is to shield the copper from solvent and potential external ligands.[6]

Conclusions: Extensive experimental and theoretical work has led to a consistent picture of a blue copper site. The His-His-Cys triplet that makes up the trigonal plane is positioned to bind the metal, while the axial interactions may be easily forced into alternate conformers. The ligand sidechains, as well as the rest of the protein framework, also exist to sequester the metal from undesired ligands such as solvent, ions, and small

molecules. In keeping the solvent from the copper, but only by a small distance, blue copper proteins simultaneously minimize the reorganization energy while maximizing coupling. These two factors together allow for the rapidest possible electron transfer in biological copper systems.

Figure 1.1: X-ray structure of the copper ligation sphere in *P. denitrificans* amicyanin. The Cys-His-Met ligands are located closely to each other along the Northern loop. The copper is represented by the ball.

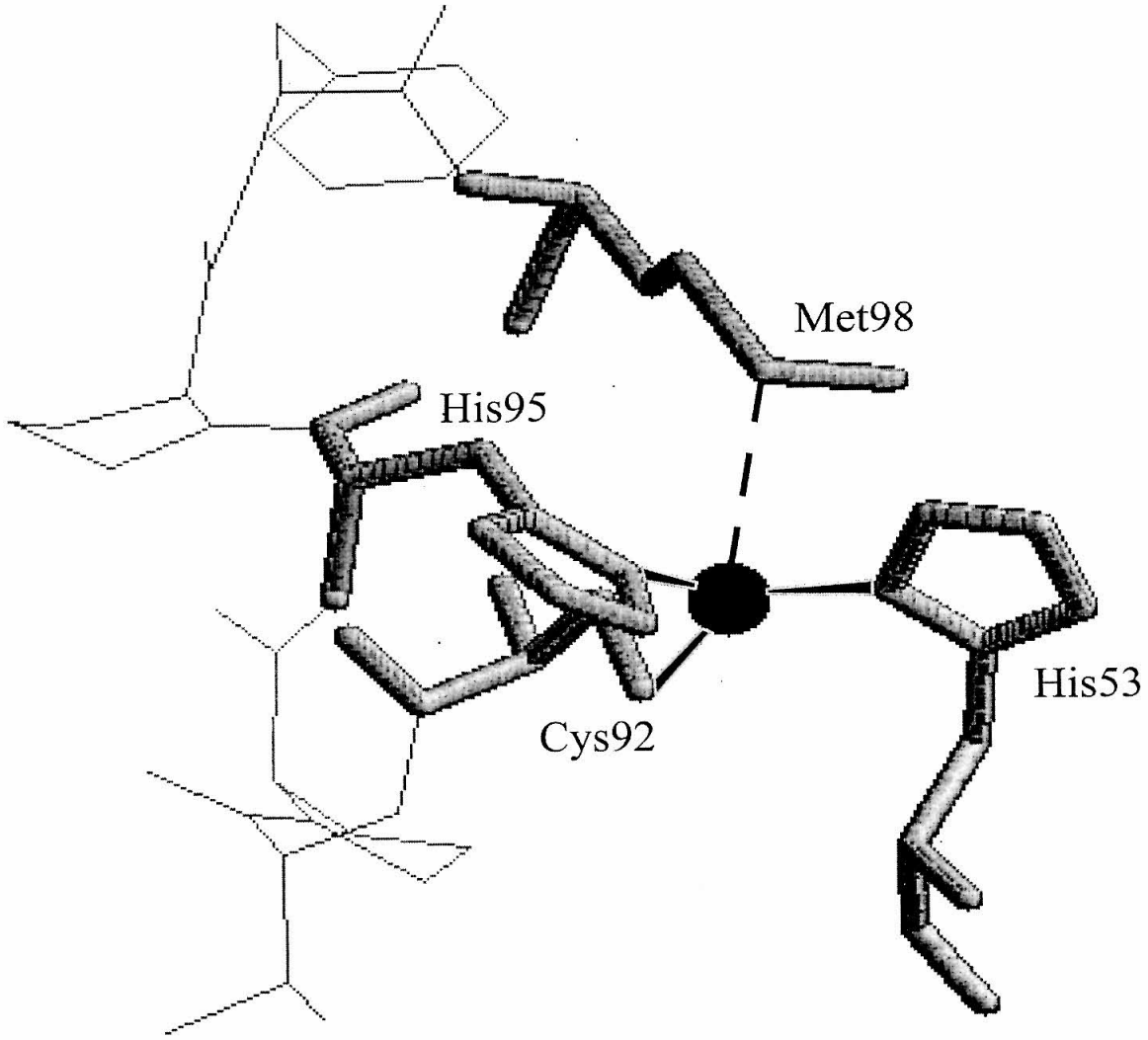
Met98
His95
His53
Cys92

Figure 1.2: Equilibria of the C-terminal histidine ligand. In the reduced form, the imidazole protonates, and then rotates to hydrogen bond with a nearby carbonyl.

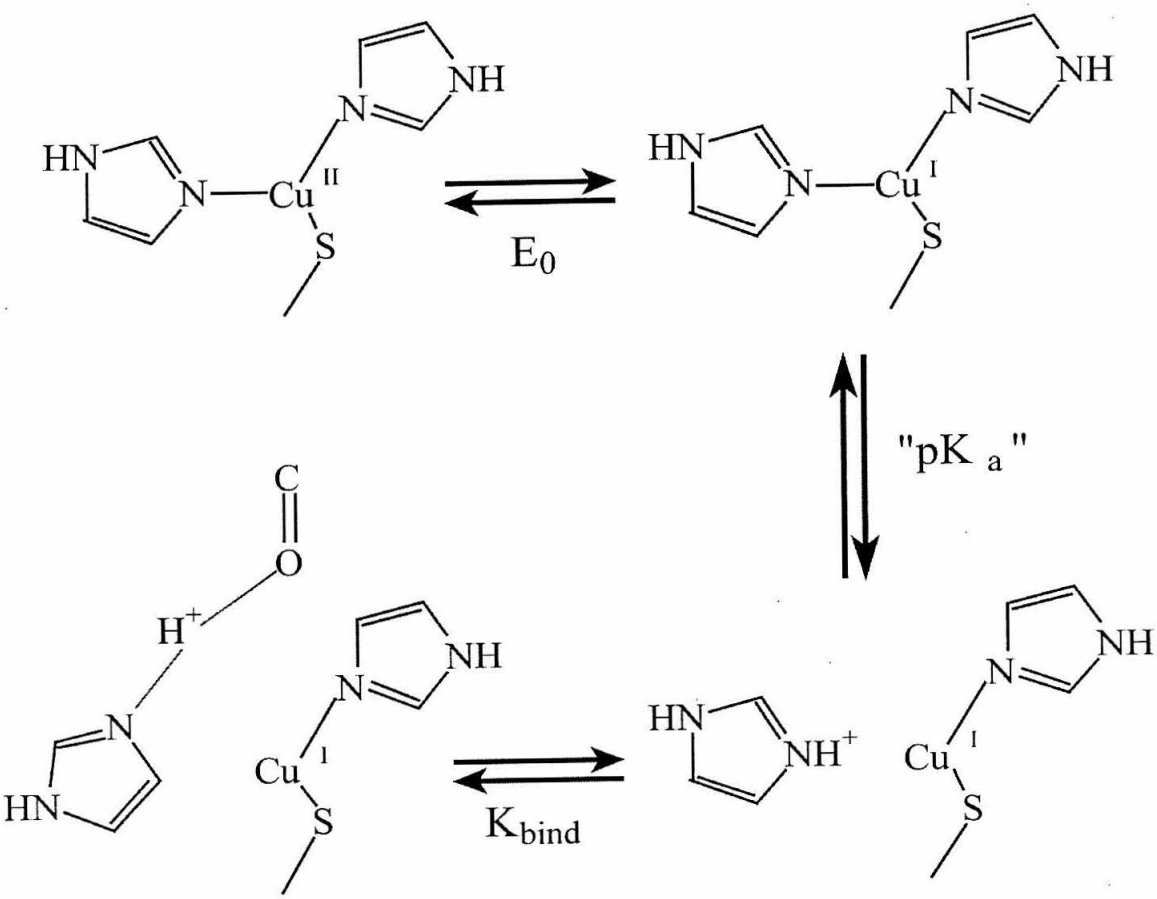
HN
N
Cu II
S
NH
N
E0
HN
N
Cu I
S
NH
N
"pK a"
C
O
H+
HN
N
Cu I
S
NH
N
Kbind
HN
NH+
Cu I
S
NH
N

Figure 1.3: Details of the hydrogen bond network that holds the copper site together in *Pseudomonas aeruginosa* azurin. (Figure is generous gift of Prof. Brian Crane.)

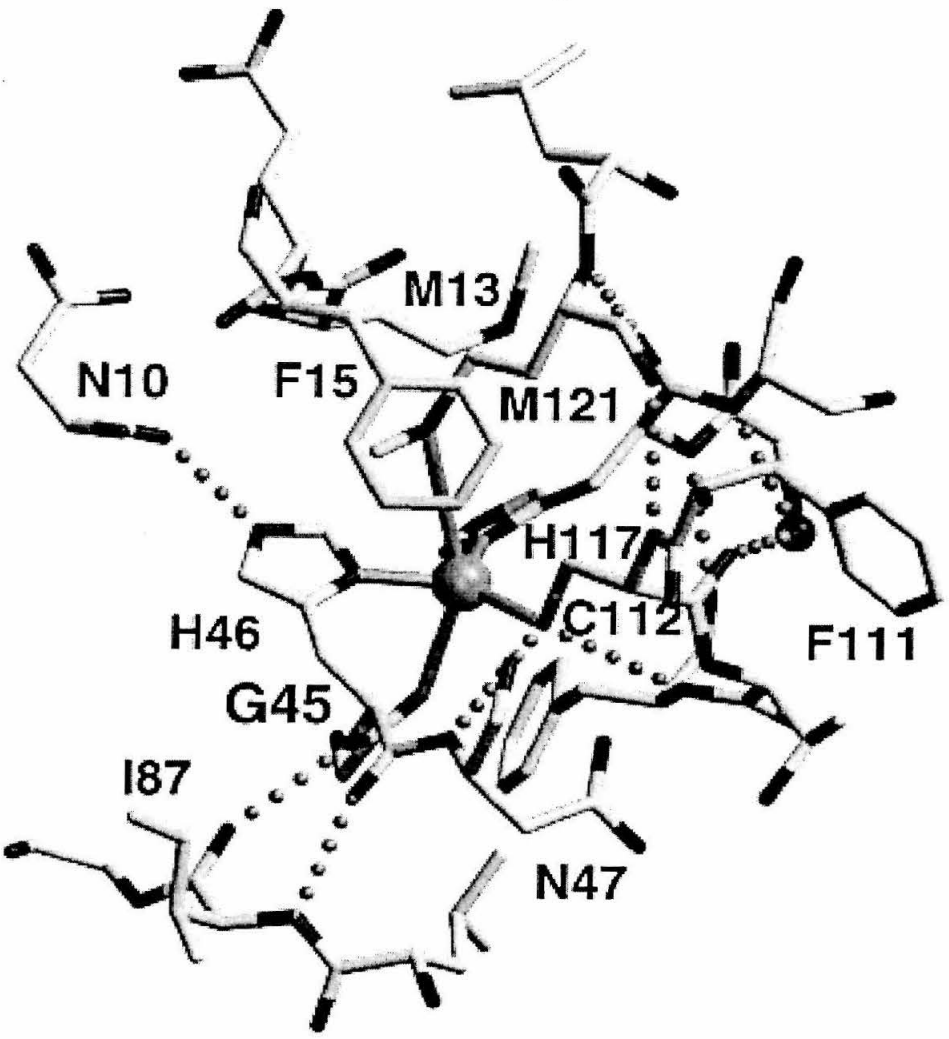
Pseudomonas aeruginosa Azurin
M13
N10
F15
M121
H117
H46
C112
F111
G45
I87
N47

Figure 1.4: Detail of asparagine hydrogen bonds to the cysteine and threonine of the Northern loop. These bonds act are believed to act as a clasp, holding the ligand loop against the rest of the protein. Taken from the crystal structure of *P. denitrificans* amicyanin. Solid lines indicate covalent bonds, dashed lines indicate hydrogen bonds.

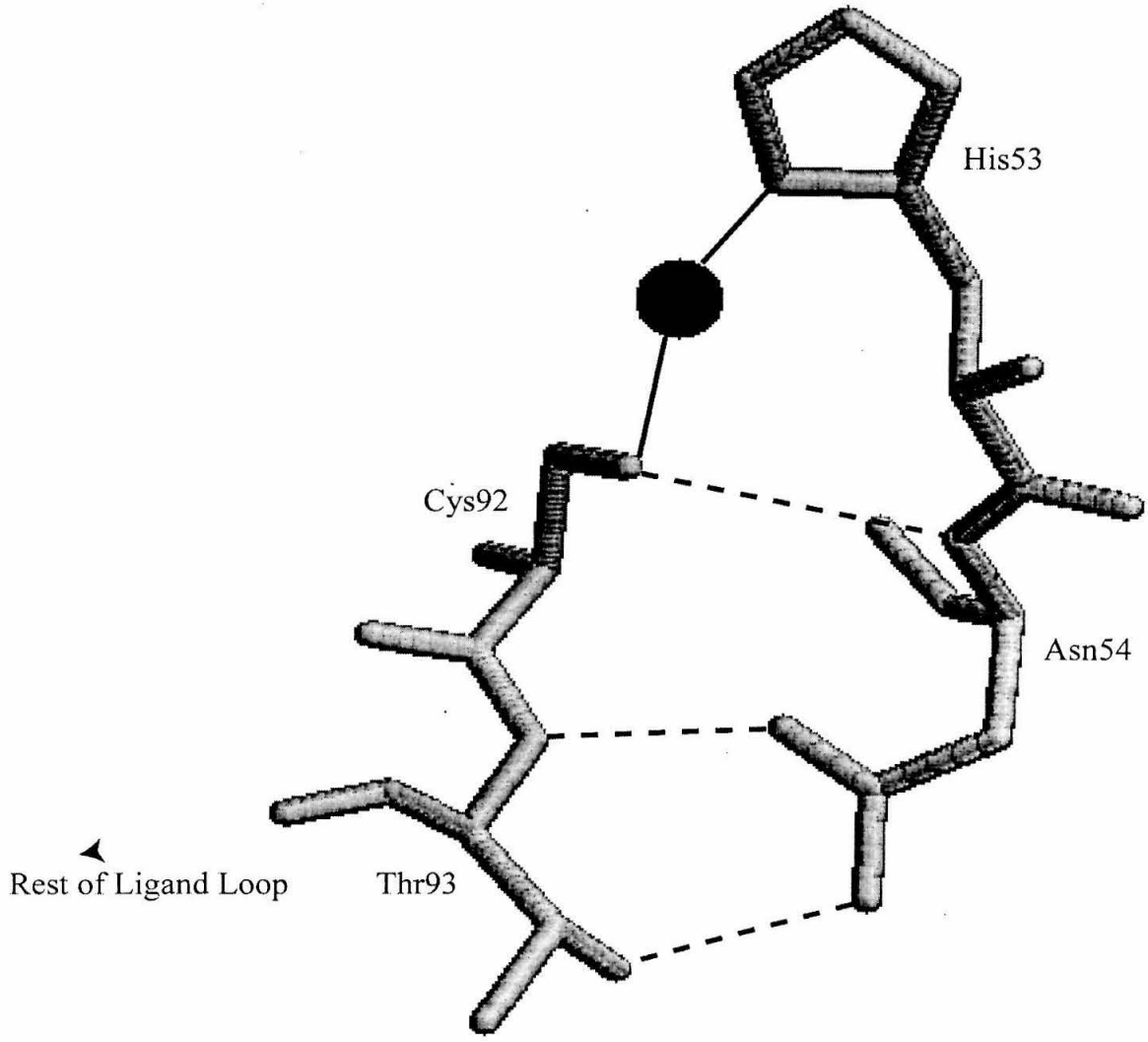
His53
Cys92
Asn54
Rest of Ligand Loop
Thr93

Figure 1.5: Region of the crystal structure of M121H azurin at alkaline pH, exhibiting the the apical imidazole pulling the copper out of the ligand plane. Notice that the carbonyl of Gly45, normally considered a ligand, is quite distant.

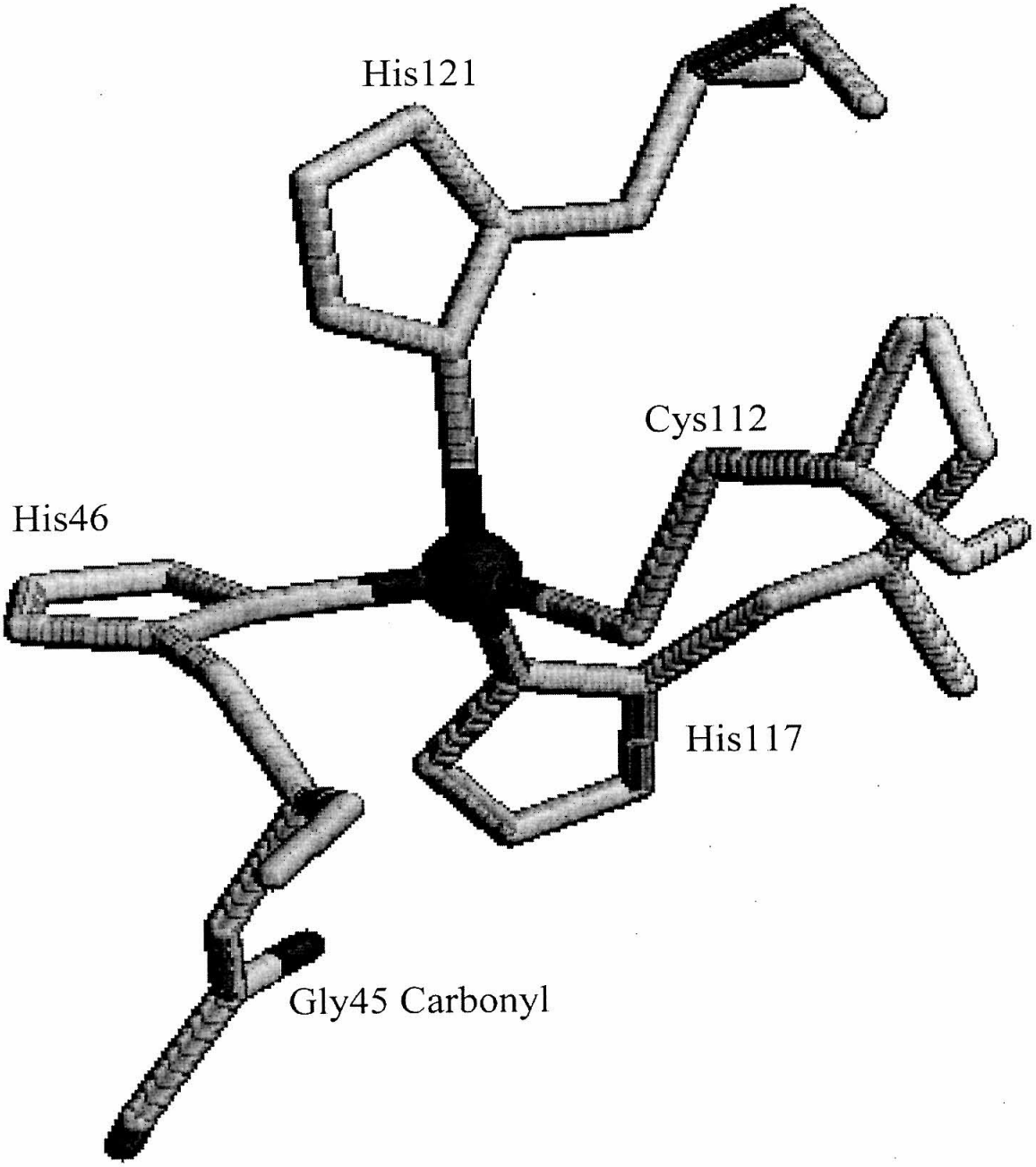
His121
Cys112
His46
His117
Gly45 Carbonyl

1)Frausto da Silva, J. R. R.; Wiliams, R. J. P. *The biological chemistry of the elements*; Oxford University Press: Oxford, 1991.

2)Bertini, I.; H.B., G.; Lippard, S. J.; Valentine, J. S. *Bioinorganic chemistry*; University Science Books: Mill Valley, Calif., 1994.

3)Winkler, J. R.; Di Bilio, A. J.; Farrow, N. A.; Richards, J. H.; Gray, H. B. *Pure Appl. Chem.* **1999**, *71*, 1753-1764.

4)McConnell, H. M. *J. Chem. Phys.* **1961**, *35*, 508-515.

5)Mines, G. A.; Bjerrum, M. J.; Hill, M. G.; Casimiro, D. R.; Chang, I. J.; Winkler, J. R.; Gray, H. B. *J. Am. Chem. Soc.* **1996**, *118*, 1961-1965.

6)Gray, H. B.; Malmström, B. G.; Williams, R. J. P. *JBIC* **2000**, Available online.

7)Solomon, E. I.; Penfield, K. W.; Gewirth, A. A.; Lowery, M. D.; Shadle, S. E.; Guckert, J. A.; LaCroix, L. B. *Inorg. Chim. Acta* **1996**, *243*, 67-78.

8)Adman, E. T. *Adv. Prot. Chem.* **1991**, *42*, 145-197.

9)Winkler, J. R.; Wittung-Stafshede, P.; Leckner, J.; Malmström, B. G.; Gray, H. B. *Proc. Natl. Acad. Sci. USA* **1997**, *94*, 4246-4249.

10)Malmström, B. G. *Two Forms of Copper in Copper-Containing Oxidases*; King, T. E., Mason, H. S. and Morrison, M., Ed.; Wiley: New York, 1965; Vol. 1, pp 207-216.

11)Di Bilio, A. J.; Hill, M. G.; Bonander, N.; Karlsson, B. G.; Villahermosa, R. M.; Malmström, B. G.; Winkler, J. R.; Gray, H. B. *J. Am. Chem. Soc.* **1997**, *119*, 9921-9922.

12)Skov, L. K.; Pascher, T.; Winkler, J. R.; Gray, H. B. *J. Am. Chem. Soc.* **1998**, *120*, 1102-1103.

13)Garrett, T. P. J.; Clingeleffer, D. J.; Guss, J. M.; Rogers, S. J.; Freeman, H. C. *J. Biol. Chem.* **1984**, *259*, 2822-2825.

14)Nar, H.; Messerschmidt, A.; Huber, R.; Vandekamp, M.; Canters, G. W. *FEBS Lett.* **1992**, *306*, 119-124.

15)Shepard, W. E. B.; Kingston, R. L.; Anderson, B. F.; Baker, E. N. *Acta Cryst. D* **1993**, *49*, 331-343.

16)Gross, E. L.; Draheim, J. E.; Curtiss, A. S.; Crombie, B.; Scheffer, A.; Pan, B.; Chiang, C.; Lopez, A. *Arch. Biochem. Biophys.* **1992**, *298*, 413-419.

17)Guss, J. M.; Harrowell, P. R.; Murata, M.; Norris, V. A.; Freeman, H. C. *J. Mol. Biol.* **1986**, *192*, 361-387.

18)Lommen, A.; Canters, G. W. *J. Biol. Chem.* **1990**, *265*, 2768-2774.

19)Lommen, A.; Pandya, K. I.; Koningsberger, D. C.; Canters, G. W. *Biochim. Biophys. Acta* **1991**, *1076*, 439-447.

20)Dennison, C.; Kohzuma, T.; McFarlane, W.; Suzuki, S.; Sykes, A. G. *J. Chem. Soc. Chem. Comm.* **1994**, *5*, 581-582.

21)den Blaauwen, T.; Canters, G. W. *J. Am. Chem. Soc.* **1993**, *115*, 1121-1129.

22)Ryde, U.; Olsson, M. H. M. *Submitted* **2000**.

23)Baker, E. N. *J. Mol. Biol.* **1988**, *203*, 1071-1095.

24)Nar, H.; Messerschmidt, A.; Huber, R.; van de Kamp, M.; Canters, G. W. *J. Mol. Biol.* **1991**, *221*, 765-772.

25)Messerschmidt, A. *Struct Bonding* **1998**, *90*, 37-68.

26)Bonander, N.; Vänngård, T.; Tsai, L.-C.; Langer, V.; Nar, H.; Sjölin, L. *Proteins* **1997**, *27*, 385-394.

27)Moratal, J. M.; Romero, A.; Salgado, J.; Perales-Alarcón, A.; Jiménez, H. R. *Eur. J. Biochem.* **1995**, *228*, 653-657.

28)Nar, H.; Huber, R.; Messerschmidt, A.; Filippou, A. C.; Barth, M.; Jaquinod, M.; van de Kamp, M.; Canters, G. W. *Eur. J. Biochem.* **1992**, *205*, 1123-1129.

29)Baker, E. N. *J. Mol. Biol.* **1988**, *203*, 1071-1095.

30)Shepard, W. E. B.; Anderson, B. F.; Lewandoski, D. A.; Norris, G. E.; Baker, E. N. *J. Am. Chem. Soc.* **1990**, *112*, 7817-7819.

31)Blackwell, K. A.; Anderson, B. F.; Baker, E. N. *Acta Cryst. D* **1994**, *50*, 263-270.

32)Guss, J. M.; Bartunik, H. D.; Freeman, H. C. *Acta Cryst. B* **1992**, *48*, 790-811.

33)Guss, J. M.; Harrowell, P. R.; Murata, M.; Norris, V. A.; Freeman, H. C. *J. Mol. Biol.* **1986**, *192*, 361-387.

34)Church, W. B.; Guss, J. M.; Potter, J. J.; Freeman, H. C. *J. Biol. Chem.* **1986**, *261*, 234-237.

35)Inoue, T.; Sugawara, H.; Hamanaka, S.; Tsukui, H.; Suzuki, E.; Kohzuma, T.; Kai, Y. *Biochemistry* **1999**, *38*, 6063-6069.

36)Kohzuma, T.; Inoue, T.; Yoshizaki, F.; Sasakawa, Y.; Onodera, K.; Nagamoto, S.; Kitagawa, T.; Uzawa, S.; Isobe, Y.; Sugimura, Y.; Gotowda, M.; Kai, Y. *J. Biol. Chem.* **1999**, *274*, 11817-11823.

37)Petratos, K.; Dauter, Z.; Wilson, K. S. *Acta Cryst. B* **1988**, *44*, 628-636.

38)Vakoufari, E.; Wilson, K. S.; Petratos, K. *FEBS Letters* **1994**, *347*, 203-206.

39)Libeu, C. A. P.; Kukimoto, M.; Nishiyama, M.; Horinuchi, S.; Adman, E. T. *Biochemistry* **1997**, *36*, 13160-13179.

40)Inoue, T.; Nishio, N.; Suzuki, S.; Kataoka, K.; Kohzuma, T.; Kai, Y. *J. Biol. Chem.* **1999**, *274*.

41)Walter, R. L.; Ealick, S. E.; Friedman, A. M.; Blake II, R. C.; Proctor, P.; Shoham, M. *J. Mol. Biol.* **1996**, *263*, 730-751.

42)Harvey, I.; Hao, Q.; Duke, E. M. H.; Ingledew, W. J.; Hasnain, S. S. *Acta Cryst. D* **1998**, *54*, 629-635.

43)Botuyan, M. V.; Toy-Palmer, A.; Chung, J.; Blake II, R. C.; Beroza, P.; Case, D. A.; Dyson, H. J. *J. Mol. Biol.* **1996**, *263*, 752-767.

44)Messerschmidt, A.; Ladenstein, R.; Huber, R.; Bolognesi, M.; Avigliano, L.; Petruzzelli, R.; Rossi, A.; Finazzi-Agrò, A. *J. Mol. Biol.* **1992**, *224*, 179-205.

45)Messerschmidt, A.; Luecke, H.; Huber, R. *J. Mol. Biol.* **1993**, *230*, 997-1014.

46)Hoitink, C. W. G.; Canters, G. W. *J. Biol. Chem.* **1992**, *267*, 13836-13842.

47)Dong, S.; Ybe, J. A.; Hecht, M. H.; Spiro, T. G. *Biochemistry* **1999**, *38*, 3379-3385.

48)Olsson, M. H. M.; Ryde, U.; Roos, B. O. *Prot. Sci.* **1998**, *7*, 2659-2668.

49)Gray, H. B.; Malmström, B. G. *Comm. Inorg. Chem.* **1983**, *2*, 203-209.

50)Guckert, J. A.; Lowery, M. D.; Solomon, E. I. *J. Am. Chem. Soc.* **1995**, *117*, 2817-2844.

51)LaCroix, L. B.; Shadle, S. E.; Wang, Y. N.; Averill, B. A.; Hedman, B.; Hodgson, K. O.; Solomon, E. I. *J. Am. Chem. Soc.* **1996**, *118*, 7755-7768.

52)Pierloot, K.; De Kerpel, J. O. A.; Ryde, U.; Olsson, M. H. M.; Roos, B. O. *J. Am. Chem. Soc.* **1998**, *120*, 13156-13166.

53)Lowery, M. D.; Solomon, E. I. *Inorg. Chim. Acta.* **1992**, *198-200*, 233-243.

54)Adman, E. T.; Turley, S.; Bramson, R.; Petratos, K.; Banner, D.; Tsernoglou, D.; Beppu, T.; Watanabe, H. *J. Biol. Chem.* **1989**, *264*, 87-99.

55)Messerschmidt, A.; Prade, L.; Kroes, S. T.; Sanders-Loehr, J.; Huber, R.; Canters, G. W. *Proc. Natl. Acad. Sci. USA* **1998**, *95*, 3443-3448.

56)Buning, C.; Canters, G. W.; Comba, P.; Dennison, C.; Jeuken, L.; Melter, M.; Sanders-Loehr, J. *J. Am. Chem. Soc.* **2000**, *122*, 204-211.

57)Bonander, N.; Vänngård, T.; Tsai, L.; Langer, V.; Nar, H.; Sjölin, L. *Proteins* **1997**, *27*, 385-394.

58)Shepard, W. E. B.; Anderson, B. F.; Lewandoski, D. A.; Norris, G. E.; Baker, E. N. *J. Am. Chem. Soc.* **1990**, *112*, 7817-7819.

59)Ryde, U.; Olsson, M. H. M.; Pierloot, K.; Roos, B. O. *J. Mol. Biol.* **1996**, *261*, 586-596.

60)Kitajima, N.; Fujisawa, K.; Moro-oka, Y. *J. Am. Chem. Soc.* **1990**, *112*, 3210-3212.

61)Qiu, D.; Kilpatrick, L. T.; Kitajima, N.; Spiro, T. G. *J. Am. Chem. Soc.* **1994**, *116*, 2585-2590.

62)Kitajima, N.; Fujisawa, K.; Tanaka, M.; Moro-oka, Y. *J. Am. Chem. Soc.* **1992**, *114*, 9232-9233.

63)Leckner, J.; Bonander, N.; Wittung-Stafshede, P.; Malmström, B. G.; Karlsson, B. G. *Biochim. Biophys. Acta* **1997**, *1342*, 19-27.

64)Luo, J. ; California Institute of Technology: Pasadena, CA, 1997, pp 67-110.

65)Wittung-Stafshede, P.; Gomez, E.; Öhman, A.; Aasa, R.; Villahermosa, R. M.; Leckner, J.; Karlsson, B. G.; Sanders, D.; Fee, J. A.; Winkler, J. R.; Malmström, B. G.; Gray, H. B.; Hill, M. G. *Biochem. Biophys. Acta* **1998**, *1388*, 437-443.

66)DeBeer, S.; Wittung-Stafshede, P.; Leckner, J.; Karlsson, B. G.; Winkler, J. R.; Gray, H. B.; Malmström, B. G.; Solomon, E. I.; Hedman, B.; Hodgson, K. O. *Inorg. Chim. Acta* **2000**, *297*, 278-282.

67)La Rosa, C.; Milardi, D.; Grasso, D.; Guzzi, R.; Sportelli, L. *J. Phys. Chem.* **1995**, *99*, 14864-14870.

68)Ubbink, M.; Lian, L. Y.; Modi, S.; Evans, P. A.; Bendall, D. S. *Eur. J. Biochem.* **1996**, *242*, 132-147.

69)Lumry, R.; Eyring, H. *J. Phys. Chem.* **1953**, *58*, 110-120.

70)van Pouderoyen, G.; Andrew, C. R.; Loehr, T. M.; Sanders-Loehr, J.; Mazumdar, S.; Hill, H. A. O.; Canters, G. W. *Biochemistry* **1996**, *35*, 1397-1407.

71)Bonander, N.; Karlsson, B. G.; Vänngård, T. *Biochemistry* **1996**, *35*, 2429-2436.

Chapter 2:

Electrochemistry of Amicyanin

Background:

While the rack effect is supported by the observations in the previous chapter, much of the information is qualitative, or quantitative on a scale that is not very gradual. In order to properly quantify the rack effect, the hydrogen-bonding network around the active site needs to be altered in a minimalist manner that does not result in copper loss (such as alteration of the conserved asparagine) or dramatic rearrangements of the copper site itself (such as ligand mutations or metal substitution).

A reaction that is well suited as a reporter of the rack effect is the protonation of the C-terminal histidine residue. In the reduced state, poplar plastocyanin[1] and *A. faecalis S-6* pseudoazurin[2] crystal structures have shown that this histidine ligand protonates, detaches from the copper, and rotates into another conformer (Figure 2.1). The same occurrences were observed by NMR for *P. versutus* amicyanin[3]. It is becoming apparent that other proteins of the family, such as CBP[4], also exhibit this behavior, but at much lower pH. Reexamination of previous data reveals discrepancies that may be easily explained by histidine ligand protonation[5]. In fact, the pKa's range from 7.5 (*P. denitrificans* amicyanin)[6] to 3.8 (CBP), although lower values are likely to exist. One of the conclusions from the introduction is that a function of the rack is to hold the ligands in the proper orientation for metal binding, especially copper(I). Thus, the measurement and adjustment of this pK_a would be one way to quantify the rack.

Shortly after the discovery[7] and electrochemical characterization of plastocyanin[8] by Katoh, Williams and coworkers suggested the pH-dependent reduction potential was

due to the protonation of the C-terminal histidine ligand[9]. This suggestion was subsequently supported by the NMR measurements of Markley in 1975[10]. The x-ray structure was solved in 1978 by Freeman[11], but low-pH forms that clearly demonstrated the histidine conformer weren't available until 1986[1]. Sykes has spent much time elaborating on the process through redox reactions with numerous small inorganic complexes[12]. It was found that the protonated forms were unreactive with these compounds, which is expected because three-coordinate copper should have a high reduction potential. In the 1980s and 90s, more proteins that exhibited redox inactivity at low pH were discovered. When the database of blue copper proteins had grown, the question of what was responsible for the differences in protonation became more tractable. Sykes first proposed that the number of amino acids in the loop separating the cysteine ligand from the protonating histidine controlled imidazole protonation (Table 2.1)[13,14]. Freeman later suggested that the key feature was not the number of residues, but the number of hydrogen bonds to the thiolate of the cysteine ligand[15]; all the blue copper proteins have a hydrogen bond to the cysteine sulfur from the amide of the

Table 2.1: Sequences of the Northern loop regions of several blue copper proteins.

Amicyanin*	Cys	Thr	Pro			His	Pro	Phe			Met
Plastocyanin*	Cys	Ser	Pro			His	Gln	Gly	Ala	Gly	Met
Pseudoazurin*	Cys	Thr	Pro			His	Tyr	Ala	Met	Gly	Met
CBP	Cys	Asn	Phe	Pro	Gly	His	Cys	Gln	Ser	Gly	Met
Azurin	Cys	Thr	Phe	Pro	Gly	His	Ser		Ala	Leu	Met
Rusticyanin	Cys	Gln	Ile	Pro	Gly	His	Ala	Ala	Thr	Gly	Met

* protonates with a $pK_a > 4.5$

conserved asparagine that follows the N-terminal histidine ligand. However, in the forms that do not protonate (or rather, protonate at very low pH), a second hydrogen bond is linked to the thiolate. The origin of this hydrogen bond is the amide proton of the second amino acid after the cysteine (Cys +2, Figure 2.2). The species that protonate possess a proline at this position and thus no amide proton.

Mutants of the pseudoazurin from *Alcaligenes faecalis* have been made, with the proline changed to alanine and isoleucine[16]. Crystal structures indicate that the alanine allows a water into the cavity, while isoleucine's sidechain prohibits the entry of water[17]. The amide of the isoleucine forms the predicted hydrogen bond, but pH-dependent properties of the mutants have not been investigated. The amide proton of the alanine mutant points between the water oxygen and the cysteine thiol. Analogous phenylalanine and alanine mutations were made in the amicyanin from *Paracoccus denitrificans,* and the properties of these variants were examined. Amicyanin has the highest pKa of these proteins, so any difficulties that arise from low-pH measurements should be best avoided in this system.

Amicyanin is a typical blue copper protein, with an absorption maximum at 596 nm[18]. The crystal structure of amicyanin (Figure 2.3) shows that it possesses a beta sandwich structure[19]. The species examined in this thesis is found in the periplasm of *Paracoccus denitrificans*. When grown on methylamine, amicyanin is expressed as a vital electron carrier in the first stage of respiration (Figure 2.4). Electrons are transferred from methylamine dehydrogenase (MADH) through amicyanin to cytochrome c551i or

c550 in a ternary complex between all three proteins[20]. The crystal structures of the MADH/amicyanin/cytochrome c551i ternary complex[21], as well as both binary complexes[22], have been solved. In the binary complexes, the cytochrome and MADH bind to the same position on amicyanin: the hydrophobic patch located near the metal site[23]. In the ternary complex, MADH occupies this position, while the cytochrome is resident further away. It is tempting to suggest that the protonation behavior of amicyanin is a regulatory gate for electron transfer and the metabolic cycle, but experiments have shown that the potential of amicyanin in the complex is pH-independent[6], disproving that hypothesis.

Methods and Materials:

Site-directed mutagenesis: Mutants were created using the Quikchange method from Stratagene. A plasmid consisting of the amicyanin gene cloned into pUC 19 was the generous gift of Victor Davidson (Figure 2.5). A typical reaction consists of 50 ng template, 125 pmol of each primer, 100 μM total dNTPs, 5 λ 10x buffer, 1 λ *Pfu turbo* polymerase (adjusted to 50 λ total volume with ddH_2O). An initial melt of x min at 95 degrees C was followed by 16 cycles of melting, annealing, and extension (30s at 95 degrees C, 1 min at 55 degrees C, 9 min at 68 degrees C). The reaction mixture was then set for a five minute extension and cooled to 4 degrees C. PCR products were analyzed on 1% agarose gel in TAE and detected by ethidium bromide staining. Digestion of the template DNA was carried out by addition of 1 λ DpnI restriction enzyme (10 U/ λ) and incubation at 37 degrees C for at least an hour. One λ of this mixture was used to

transform fifty λ of chemically-competent XL1-Blue cells by a 45 second heat shock at 42 degrees C and two minutes cooling on ice. Following this, 0.5 mL of NZY+ broth (at 42 degrees C) was added and the mixture was shaken for one hour at 37 degrees C, at which point it was plated on LB plates containing 100 μg/mL ampicillin. Approximately 16 hours later, colonies were picked from the plates and grown in 3-5 mLs LB with 100 μg/mL ampicillin. After overnight growth, these cells were collected and the DNA extracted using Qiagen spin column minipreps. DNA was eluted with water at pH 7.0 and submitted to the Caltech Sequencing Facility to confirm mutagenesis. The primers used for these mutants are in Table 2.2. F and B refer to forward and backwards primers.

Table 2.2: Primers used for site-directed mutagenesis.

P94F-F	5'-ACTATCACTGCACCTTCCATCCCTTCAT-3'
P94F-B	5'-ATGAAGGGATGGAAGGTGCAGTGATAGT-3'
P94A-F	5'-ACTATCACTGCACCGCCCATCCCTTCAT-3'
P94A-B	5'-ATGAAGGGATGGGCGGTGCAGTGATAGT-3'
M28F-F	5'-ATCGTCGTCGACATCGCCAAGTTCAAATACGAAACCCCCGAA-3'
M28F-B	5'-TTCGGGGGTTTCGTATTTGAACTTGGCGATGTCGACGACGAT-3'
M51F-F	5'-AACCGCGAGGCGTTCCCGCACAATGTCCAT-3'
M51F-B	5'-ATGGACATTGTGCGGGAACGCCTCGCGGTT-3'
P52G-F	5'-AACCGCGAGGCGATGGGGCACAATGTCCAT-3'
P52G-B	5'-ATGGACATTGTGCCCCATCGCCTCGCGGTT-3'
P52G,M51F-F	5'-AACCGCGAGGCGTTCGGGCACAATGTCCAT-3'
P52G,M51F-B	5'-ATGGACATTGTGCCCGAACGCCTCGCGGTT-3'

N54P-F	5'-AGGCGATGCCGCACCCGGTCCATTTCGT-3'
N54P-B	5'-ACGAAATGGACCGGGTGCGGCATCGCCT-3'

Protein expression and purification: Plasmid DNA was transformed by the heat-shock method into chemically competent BL21(DE3) cells from Novagen and plated on LB plates containing 100 μg/mL ampicillin, which were then incubated at 37 degrees C. Colonies were usually observed after ~ 8-12 hours, at which time one was picked and grown in 3-5 mL LB with 100 μg/mL ampicillin. These cultures were then scaled to 4 – 1 L batches and grown overnight at 30 degrees C with 100 μM $Cu(SO_4)$. The cells were induced with 300 μM IPTG, and collected after 3-4 hours by centrifugation for 10 minutes at 4 degrees C in a GSA rotor at 5000 rpm. Cell pellets were immediately resuspended in 20mL/g cells lysis buffer (0.2 M Tris, pH 7.3, .5 M sucrose, 0.5 mM EDTA,) and brought to 30 degrees C. 5mg/ g cells lysozyme was added and the solution was osmotically shocked by an equal volume of ddH_2O at 30 degrees C. This solution was stirred for 20 minutes at 30 degrees, then centrifuged at 12000 rpm in a GSA rotor. The supernatant was removed and placed in dialysis sacks (10kDa cutoff, SpectraPor). It was dialyzed against 10mM KPi pH7.0, and then concentrated by ultrafiltration methods to approximately 20 mL. The protein was oxidized with $K_3Fe(CN)_6$ or $Na_2IrCl_6 \cdot 6H_2O$, and applied to a DE52 column that had been equilibrated with the same buffer. Oxidized amicyanin clearly eluted as a blue band with continued addition of the same buffer, and purity was checked by A_{280}/A_{596} ratio and SDS-PAGE. Identities of mutants were confirmed by electrospray-MS at the Caltech Microanalytical Facility.

Electrochemistry: All electrochemistry was performed in a two-chamber cell using a standard three-electrode configuration with silver/silver chloride as reference. The reference electrode potential was calibrated using ferricyanide[24] as a standard. Edge-plane graphite (EPG) was used as a working electrode, although measurements were confirmed with a gold electrode freshly modified by aminoalkylthiols. The EPG electrode was freshly prepared for each sample by polishing in a slurry of 0.3 μ alumina and nanopure water, followed by sonication for ten minutes. The gold electrode was prepared first by polishing and sonication identical to the EPG electrode. Then, the electrode was placed in a three-electrode arrangement and repeatedly scanned from 1.6 to – 0.2 V at 1V/s in 1 M H_2SO_4 until the cyclic voltammogram was reproducible (typically 15-20 scans). At this point, the electrode was sonicated, and placed in 1 mM aminoethanethiol for one minute. After rinsing again, the electrode was then used for measurement. Platinum wire was chosen as the counter electrode. The electrodes were driven and measured by a CH instruments CHI660. Temperature dependence measurements were made in an isothermal cell, adjusted for the change in reference potential as in the literature[25]. Cyclic voltammograms were typically performed at scan rates between 1 and 200 mV/s.

UV-visible absorption spectroscopy: All measurements were made on a HP8452 spectrophotometer using a 1.000 cm pathlength cell. Blanks of the corresponding buffers were taken prior to measurements.

Results and Discussion:

Wild Type

The potentials of wild type amicyanin from *P. denitrificans* had not been reported, so direct electrochemistry was performed. The protein exhibited quasi-reversible behavior (Figure 2.6). The Faradaic current from chronoamperometry[26] experiments (Figure 2.7), i.e., the current due to a redox active species, was fit to the Cottrell equation[27] (1) to yield a diffusion constant of 3.44×10^{-6} cm^2/s, which is within the expected range for a protein of 11 kDa (Table 2.3).

$$I_C = \frac{nFAD^{1/2}C}{(\pi t)^{1/2}} \qquad (1)$$

I_c is the Faradaic current, n is the number of electrons transferred, F is Faraday's constant, A is the area of the electrode surface, D is the diffusion constant, C is the concentration of the redox-active species, and t is the time after the potential step. Cyclic voltammetry gave peak to peak separations of approximately 90 mV.

Table 2.3: Diffusion coefficients and heterogenous rate constants for blue copper proteins.

Protein	Diffusion Constant x 10^{-6} cm^2/s	k (heterogeneous et) x 10^{-3} cm/s	Reference
Parsley plastocyanin	1.3	4	28
Spinach plastocyanin	0.7 (pH 4)	2(pH 8) - 10(pH 4)	29
P. a. azurin		3.3	30
A.c. pseudoazurin	2.23	37	31
Cucumber plantacyanin		4.8,2.5	30
R.v. stellacyanin		1.3, 3.3	30
Horseradish umecyanin		2.0, 4.6	30
P.d. amicyanin (WT)	3.44	5.0	This work
P.d. amicyanin (P94F)	3.44	1.2	This work

Heterogeneous rate constants were derived from cyclic voltammograms by the method of Nicholson; the rate constant is in the middle of the range for blue copper proteins. The pH-dependent reduction potentials were fit to equation 2, which is derived for the case of a single-protonation event occurring only in the one-electron reduced state[32].

$$E_{pH} = E_{alk} + \left(\frac{RT}{F}\right)\ln\left(1 + \left(\frac{[H^+]}{K_{a,red}}\right)\right) \qquad (2)$$

In this equation, E_{pH} is the potential measured at a certain pH, E_{alk} is the value of the potential at its high pH asymptote, R is the ideal gas constant, T is the temperature, F is

Faraday's constant, $[H^+]$ is the bulk solution proton concentration, and $K_{a,red}$ is the acid dissociation constant of the histidine in the reduced copper state. The parameters derived from the data fit an alkaline potential of 265 +- 4 mV (vs. NHE) and a pK_a of 7.0 (Figure 2.8). The potentials were checked with an aminoalkylthiol-modified gold electrode. No signal was detected when surface modification was not included in the preparation of the electrode (Figure 2.9).

Scan rate dependences clearly show that an event competitive with reoxidation occurs in the protein (Figure 2.10). Cathodic peak currents were always linear with the square root of the scan rate, as expected for linear diffusion to the electrode[26], but the anodic peaks deviated from linearity at higher scan rates. The forward reaction is too fast to resolve with standard solution electrochemistry, but the return to an oxidizable species is not. It appears to be pH-dependent. The kinetics behavior cannot be properly modeled, but since the process is easily affected by scan rates around 100 mV/s, it is expected to have a time constant around a second. This is very surprising, as NMR evidence shows that the protonation/deprotonation events occur at 10^4 s^{-1} and the rotation of the imidazole ring occurs at 10^2 s^{-1}, both far faster than what is observed here[3].

<u>P94A mutant:</u>

This mutant displays a potential 120 mV higher than the wild type, and a pK_a of 6.3. Similar increases in potential were observed in the pseudoazurin mutants. The crystal structure indicates that no hydrogen is formed to the thiolate from the amide, so these

results are not surprising. The blue copper absorption peak is shifted from 596 nm to 606 nm.

P94F mutant:

The P94F mutant also has a dramatically upshifted potential of 415 mV vs. NHE. When fit, the data is consistent with a pK_a of 5.0. However, there are not enough points in the low pH region to properly assign a pK_a. The lack of points beneath pH 5.5 is due to poor response of the protein to the electrode as well as difficulties with protein stability. The cathodic wave is also quasi-reversible and diffusion-controlled similar to wild type, except that the deprotonation and religation of His95 occur at a much faster rate than wild type at the same pH (Figure 2.11). This increase in rate is observed as a larger fraction of reoxidizable reduced protein being present, i.e., the curve deviates less from the diffusion limit for any given time between the forward and the reverse scan in the P94F than the wild type. The absorption maximum shifts to 608 nm. The parallel hyperfine splitting is 95 $x10^{-4}$ cm^{-1}, while the wild type is only 74 $x10^{-4}$ cm^{-1} (Figure 2.12). The red-shift in absorption and increase in hyperfine splitting indicate that a hydrogen bond has been made to the cysteine thiolate.

These experiments support the hypothesis that a second hydrogen bond controls the stability of the imidazole in the reduced form, i.e., this interaction enhances the rack effect. However, crystallographic experiments have recently demonstrated that the plastocyanin from *Dryopteris crassirhizoma* does not undergo rearrangement in the usual pH range[33,34], despite having only one hydrogen bond and high sequence identity. In

addition, while the protonation activity has been "turned off" in the P94F mutant, it has not been clearly identified how the pK_a is tuned from 7.0 in amicyanins to 4.8 in plastocyanin. Comparisons of several crystal structures lead to a revision of Freeman's model.

As shown in Figure 2.1, there is an equilibrium coupled to the protonation/deprotonation equilibrium that involves the rotation of the imidazole ring. Crystallographic analyses reveal that, after rotation, the imidazole hydrogen bonds to the carbonyl of the residue immediately preceding the N-terminal histidine ligand (Figure 2.13). It is possible that this "docking site" affects the protonation equilibrium, leading to a combination of the two as the observed equilibrium. The major difference that the *D. crassirhizoma* plastocyanin has from its relatives is that it has a glycine (like azurin) instead of a proline (like other plastocyanins) in the appropriate position (Table 2.4). In fact, every other known plastocyanin has a proline prior to the N-terminal histidine ligand.

Table 2.4: Sequences of various blue copper before N-terminal histidine ligand.

Amicyanin	Met	Pro	His
Plastocyanin (Poplar)	Phe	Pro	His
CBP	Xxx	Met	His
Pseudoazurin	Lys	Gly	His
Azurin	Met	Gly	His
Rusticyanin	Phe	Gly	His
Plastocyanin (*Dryopteris*)	Thr	Gly	His

Not including the copper ligands, this proline undergoes the largest change in position of any residue in plastocyanin, due to an C^{γ}-*exo* to C^{γ}-*endo* isomerization[1]. The thermal factor, <B>, for Pro36 in reduced poplar plastocyanin increases monotonically from 19.8 $Å^2$ at pH 7.8 to 31.6 $Å^2$ at pH 3.8. The larger thermal factor reflects greater mobility in Pro36. It has been proposed that this disorder in the cavity allows the C-terminal histidine the freedom to reorient and hydrogen bond to the carbonyl. The thermal factors for the glycine in pseudoazurin increase from less than 7 $Å^2$ to 15 $Å^2$ upon reduction[17]. The <B> for amicyanin's proline is 10 $Å^2$ in either case[19]. The glycine for all azurins examined had thermal factors of 15 $Å^2$ or less[35,36]. *D. crassirhizoma* plastocyanin ranges from 10 to 20 $Å^2$. It is possible that these numbers increase as the pH is lowered, but whether rearrangement occurs because of high disorder or disorder occurs because of rearrangement is a chicken or the egg question until more crystallographic experiments are performed. In either case, <B> is a static measurement of disorder in the crystal which do not necessarily reflect dynamics, and as such is not that significant a statistic.

Regardless, in an attempt to mimic this behavior, the Pro52 in wild type amicyanin was changed to glycine. In addition, the methionines 28 and 51 were changed to phenylalanine in the hopes that they could help amicyanin adopt an extremely acid stable conformation, similar to rusticyanin[37]. Unfortunately, all the electrochemistry and absorption spectroscopy were identical to the wild type (Figure 2.14). This result is considered very odd, since the addition of the phenylalanines should have driven the potential much higher (similar mutations have had this effect). In addition, the mutation

analagous to Pro52Gly was made in spinach plastocyanin[38]; this change increased the reduction potential by 20 mV and strongly slowed down the reaction with its natural redox partner, photosystem I. A logical explanation is that something is occurring in the secondary structure that is not predicted by simple modeling.

It is interesting to consider the potential shifts in the P94F and P94A mutants. The approximately 400 mV reduction potential represents a large increase that is very similar to the potentials seen by Adman and coworkers[16]. They suggest that the increase is due to a loosening of the region around the copper site that allows rearrangement to a position more favored by the reduced copper[17]. The copper(I) in their crystal structures are, in fact, more trigonal than those usually seen in blue copper structures. Two other arguments raised in the introduction chapter are pertinent here: first, when *P. aeruginosa* azurin is slightly unfolded by guanidine, the reduction potential is measured to be 420 mV vs. NHE[39]. The other point is that when the two hydrogen bonds connected to the threonine in the ligand loop of *A. denitrificans* azurin are removed, the resulting reduction potential is 396 mV vs. NHE[40]. These examples accomplish the loosening of the rack by different means, but all four yield potentials of approximately 400 mV, suggesting that these states are all very similar, and confirming that one purpose of the rack effect is to lower the reduction potential of many blue copper proteins.

Summary:

Attempts to control the protonation of amicyanin by mimicking the hydrogen bonding networks of more stable blue copper proteins have been successful. The addition

of a hydrogen bond connecting the cysteine thiolate to the residue prior to the C-terminal histidine inhibits imidazole detachment from the copper. These results support Freeman's model but do not explain the nonprotonation behavior of *Dryopteris crassirhizoma* plastocyanin. The increased stability of the imidazole is reflective of the rack keeping the ligands near the metal, while the increased reduction potential shows that the area outside the metal-ligand bonds has become more flexible with the mutation of a rigid proline in the ligand loop.

Figure 2.1: Putative equilibria of the C-terminal histidine ligand in blue copper proteins. As the pH is lowered, the imidazole protonates and then rotates to hydrogen bond with the carbonyl of the residue immediately prior to the N-terminal histidine ligand.

Figure 2.2: A comparison of the crystal structures of (Top) amicyanin, (Middle) azurin, and (Bottom) CBP. Hydrogen bonds to the cysteine thiolate appear as dashed lines.

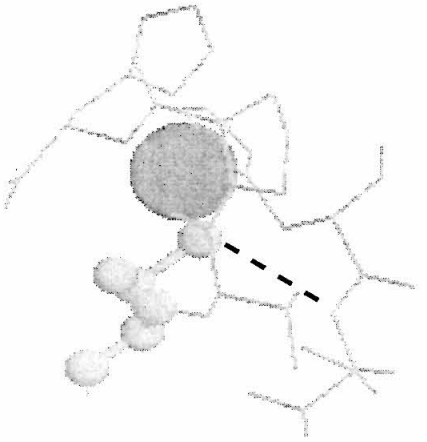

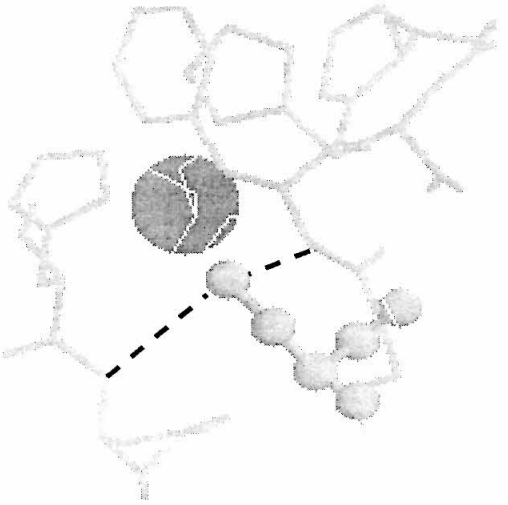

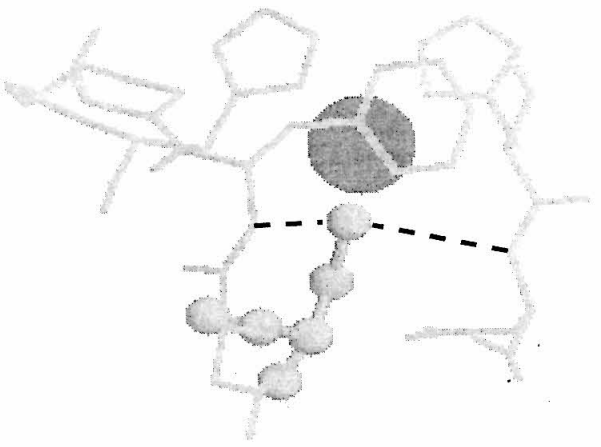

Figure 2.3: Ribbon diagram of the x-ray structure of oxidized *P. denitrificans* amicyanin. The sphere near the top left is a space-filling model of the copper atom.

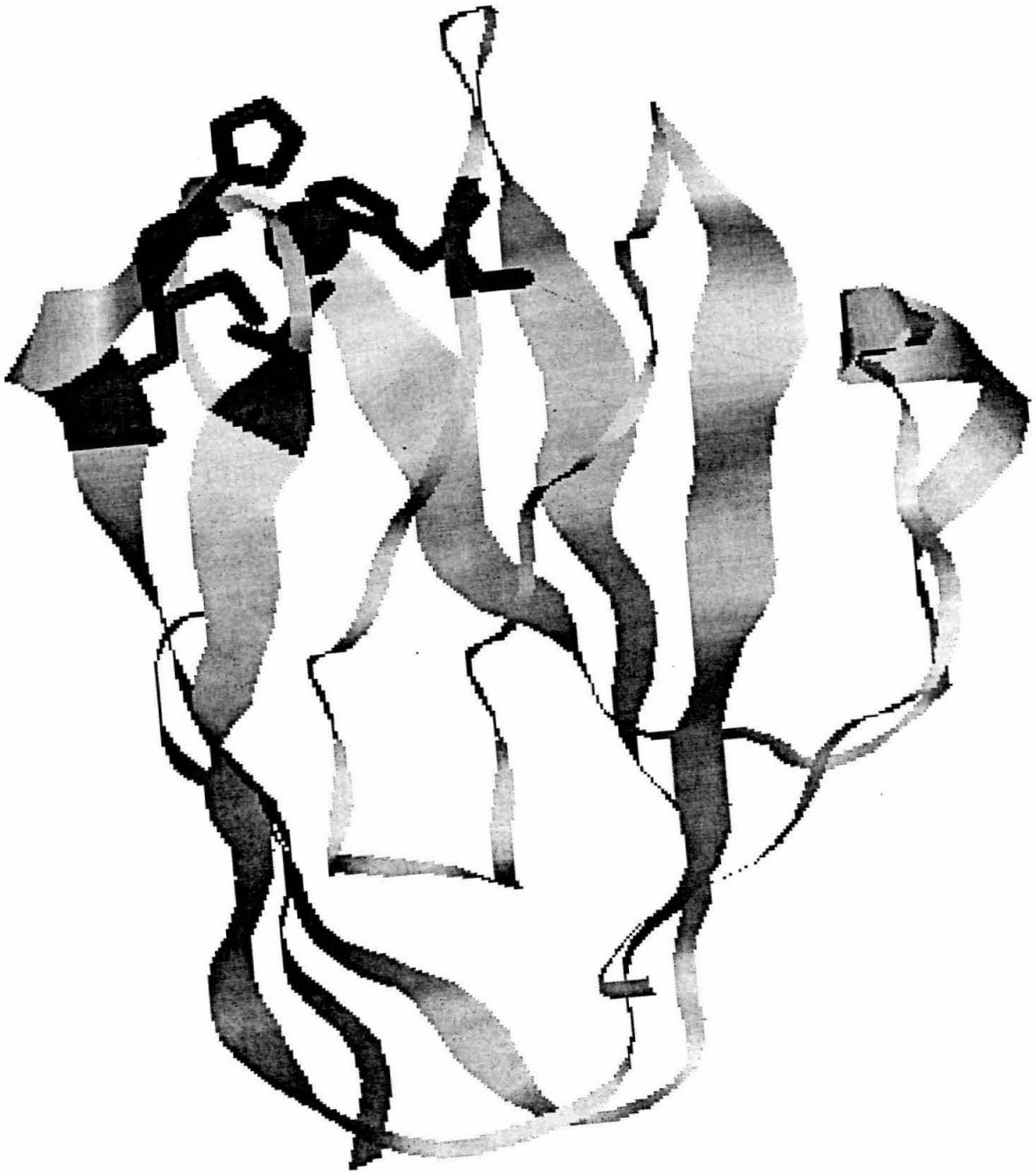

Figure 2.4: First steps of the respiratory chain in *Paracoccus denitrificans*, as induced by growth on methylamine. Methylamine dehydrogenase (MADH) transfers electrons only to amicyanin, which then gives the electrons to a variety of cytochromes c. The cytochromes are eventually oxidized by cytochrome c oxidase.

Figure 2.5: Map of the construct used for the expression of amicyanin. The amicyanin gene was ligated into a pUC 19 vector, disrupting the *lac Z* gene (dark black).

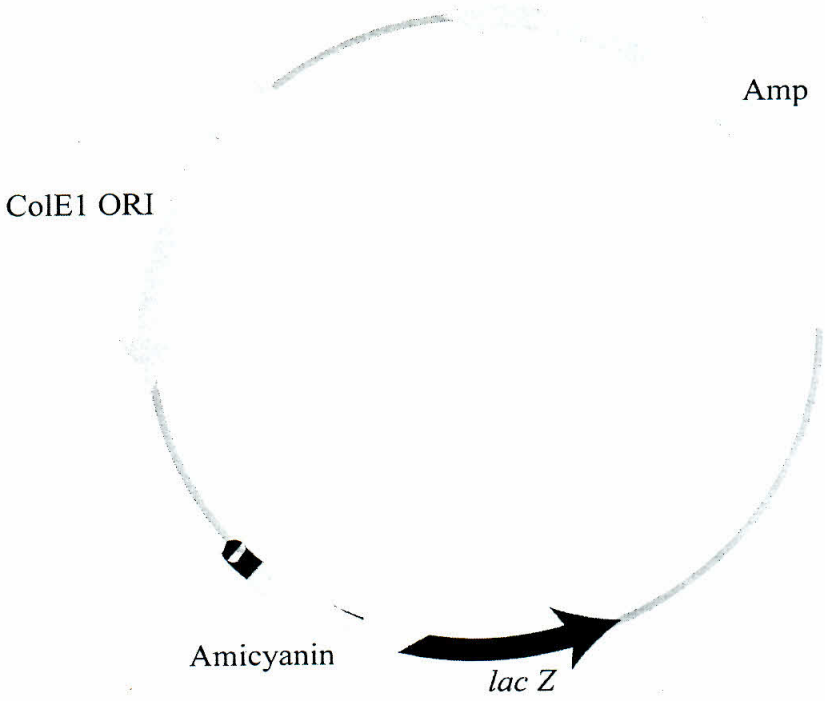
Amp
ColE1 ORI
Amicyanin
lac Z

Figure 2.6: A typical cyclic voltammogram of P94F amicyanin at a scan rate of 10 mV/s.

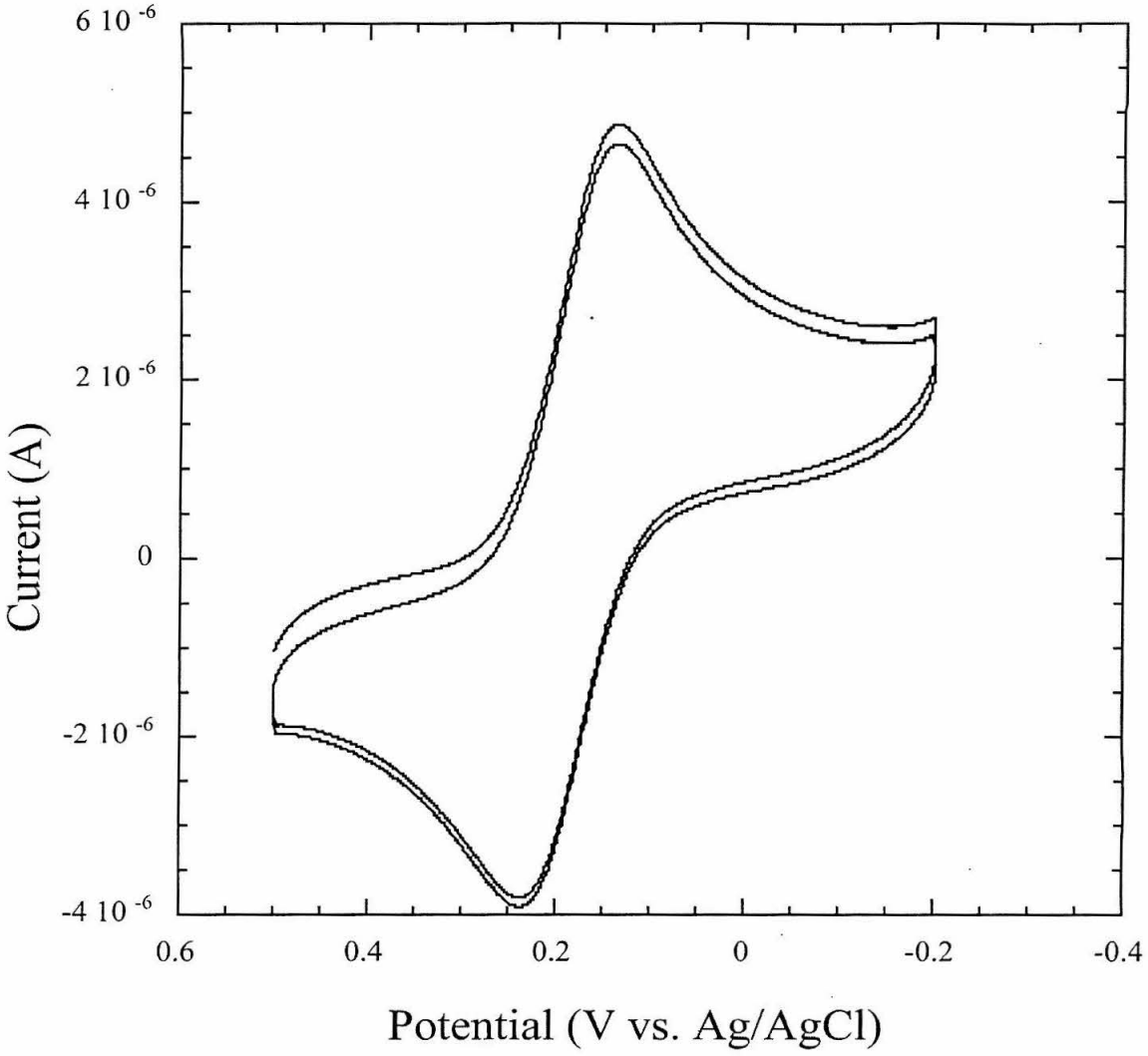
6 10 -6
4 10 -6
2 10 -6
0
-2 10 -6
-4 10 -6
Current (A)
0.6
0.4
0.2
0
-0.2
-0.4
Potential (V vs. Ag/AgCl)

Figure 2.7: Single step chronoamperometry of wild type amicyanin. Blown up inset indicates the Faradaic current, I_c, caused by the presence of the protein, which is fit to the Cottrell equation.

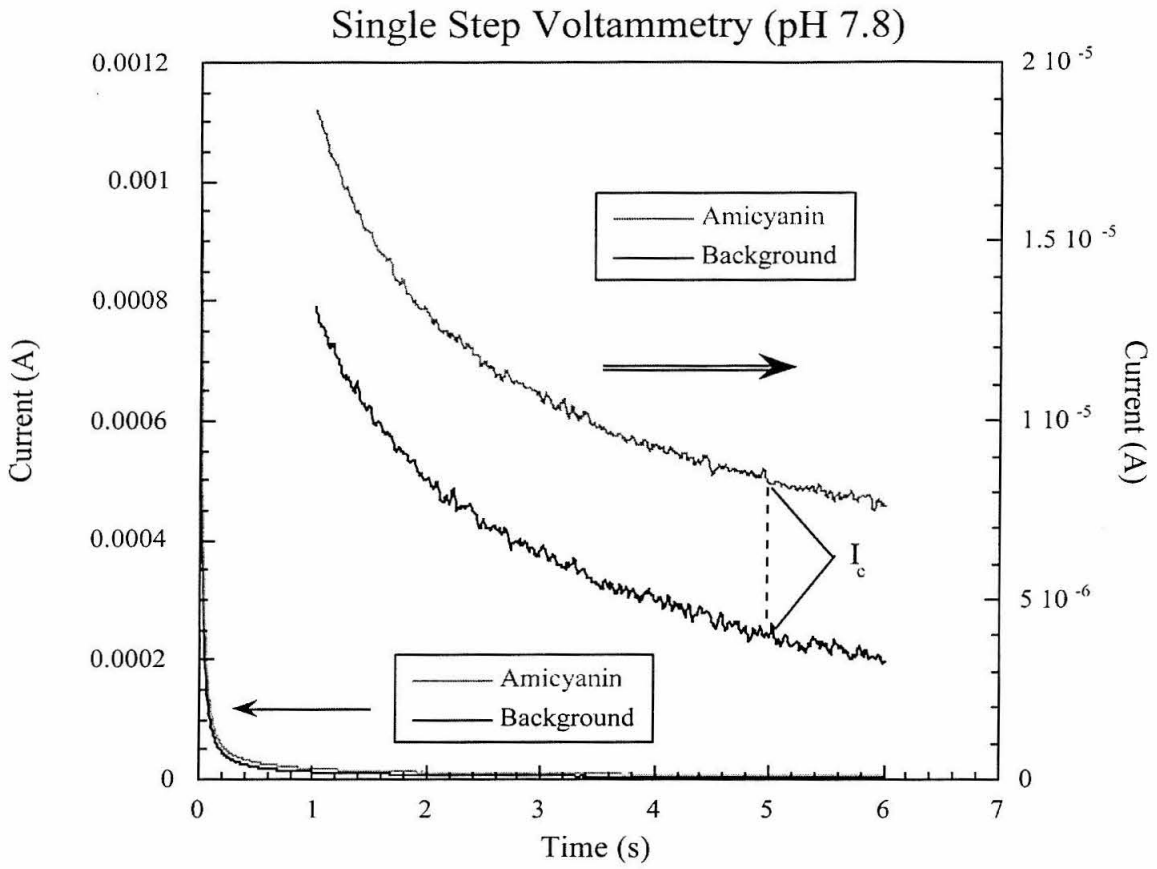
Single Step Voltammetry (pH 7.8)
Current (A)
Current (A)
Time (s)
0.0012
0.001
0.0008
0.0006
0.0004
0.0002
0
2 10 -5
1.5 10 -5
1 10 -5
5 10 -6
0
0
1
2
3
4
5
6
7
Amicyanin
Background
Amicyanin
Background
I c

Figure 2.8: Plots of E^0 vs. pH for wild type, P94F, and P94A amicyanin. The lines represent best fits to equation 2 for each protein.

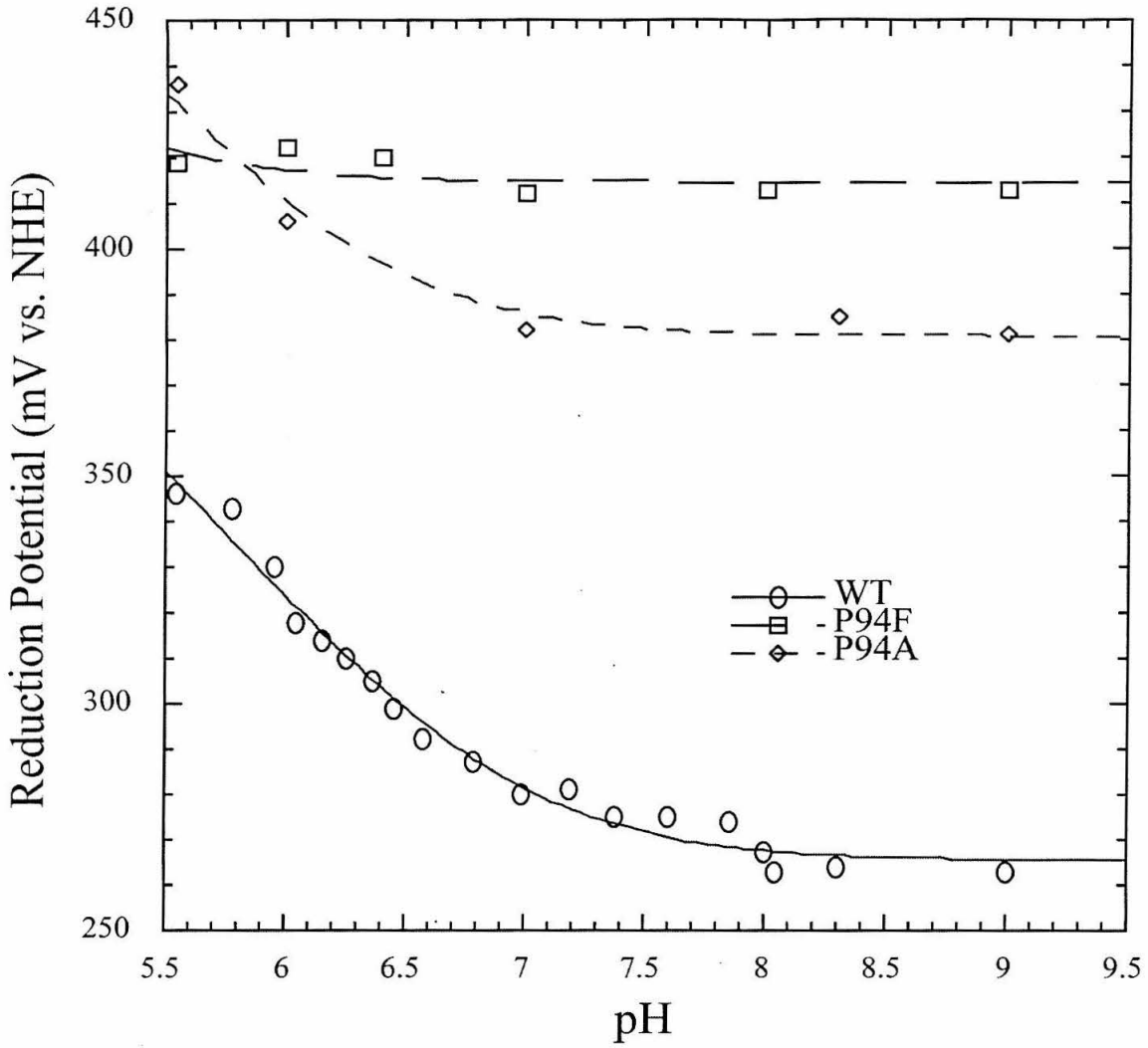
450
400
350
300
250
Reduction Potential (mV vs. NHE)
5.5
6
6.5
7
7.5
8
8.5
9
9.5
pH
WT
- P94F
- P94A

Figure 2.9: Cyclic voltammograms at a gold electrode with (black) and without (gray) aminoethanethiol treatment.

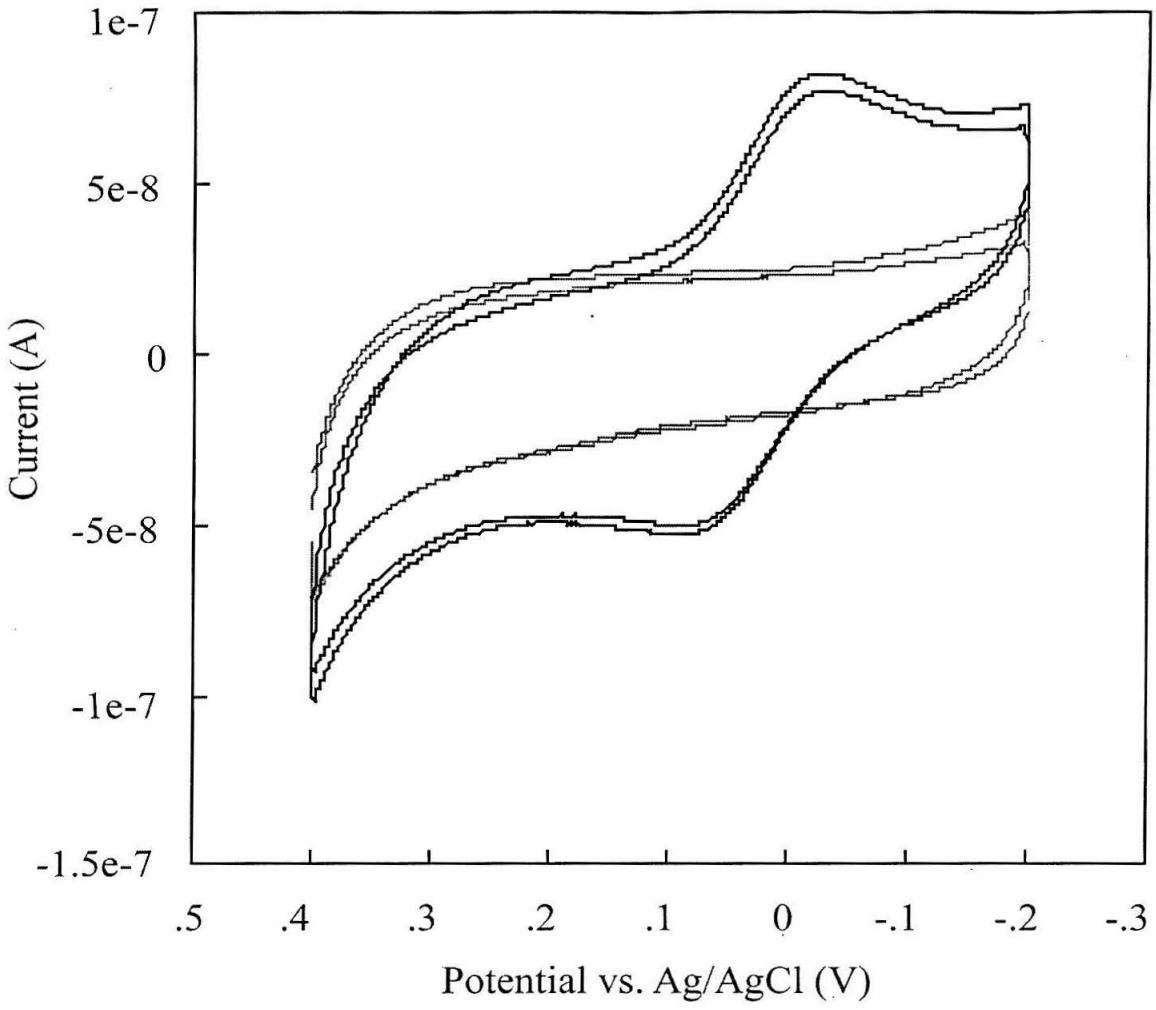
1e-7
5e-8
0
-5e-8
-1e-7
-1.5e-7
Current (A)
.5
.4
.3
.2
.1
0
-.1
-.2
-.3
Potential vs. Ag/AgCl (V)
Au electrode
Au + HSCH2CH2NH3+

Figure 2.10: Plots of the cathodic current (I_{pc}) and anodic current (I_{pa}) as a function of the square root of the scan rate for wild type amicyanin at pH 6.3. Linear behavior indicates a diffusion process that occurs linearly to the electrode face, instead of molecules diffusing radially to microsites on the electrode surface. The deviation from linearity at high scan rates and low pH for the anodic peak represent the protonation process that is competitive with reoxidation of the reduced protein.

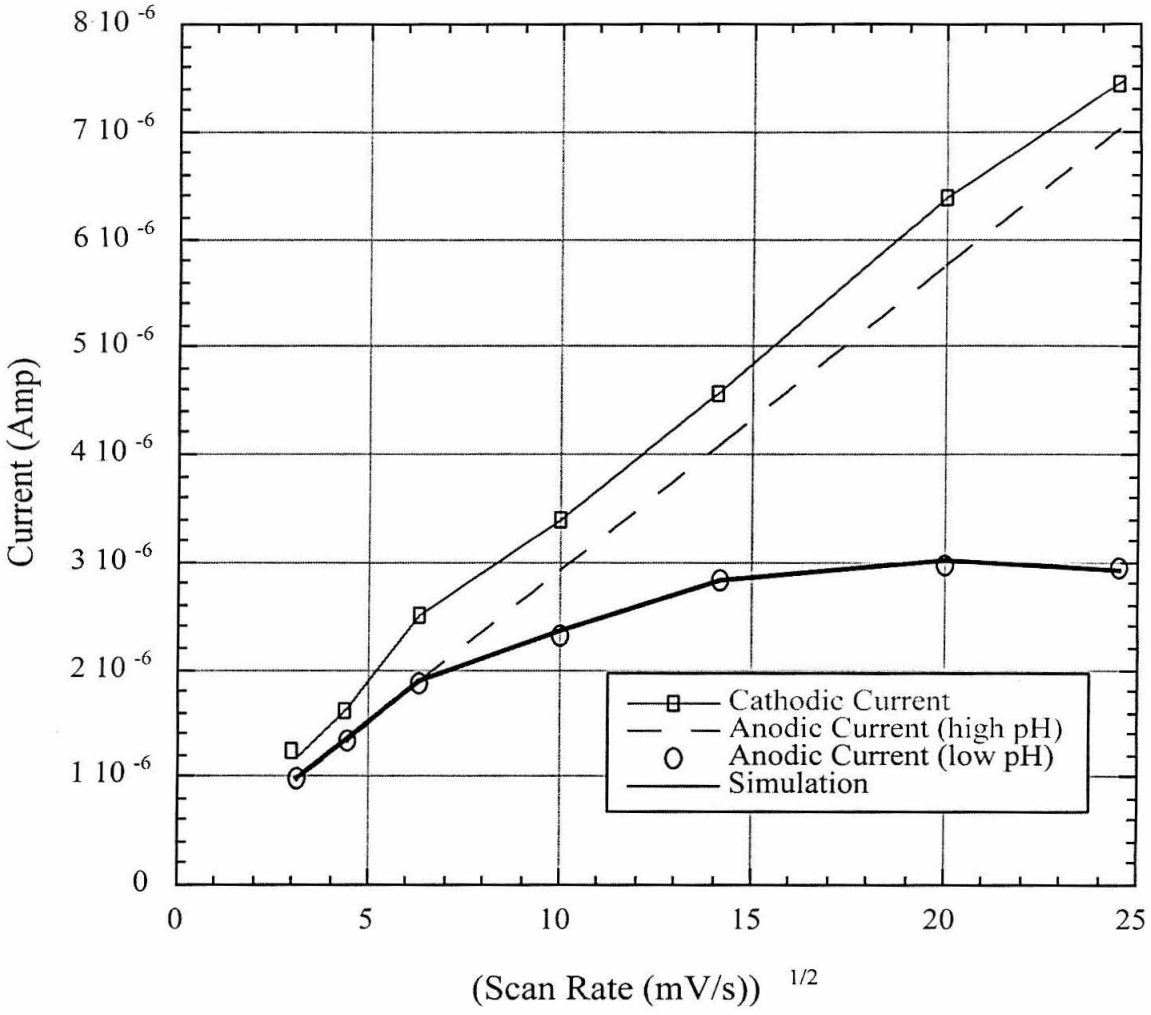
8 10 -6
7 10 -6
6 10 -6
5 10 -6
4 10 -6
3 10 -6
2 10 -6
1 10 -6
0
Current (Amp)
0
5
10
15
20
25
(Scan Rate (mV/s)) 1/2
Cathodic Current
Anodic Current (high pH)
Anodic Current (low pH)
Simulation

Figure 2.11: Plots of the cathodic current (I_{pc}) and anodic current (I_{pa}) as a function of the square root of the scan rate for P94F amicyanin at pH 6.4. Linear behavior indicates a diffusion process that occurs linearly to the electrode face, instead of molecules diffusing radially to microsites on the electrode surface. The rates for the reaction that competes with reoxidation of the reduced species, i.e., protonation, are much slower than those for wild type at the same pH.

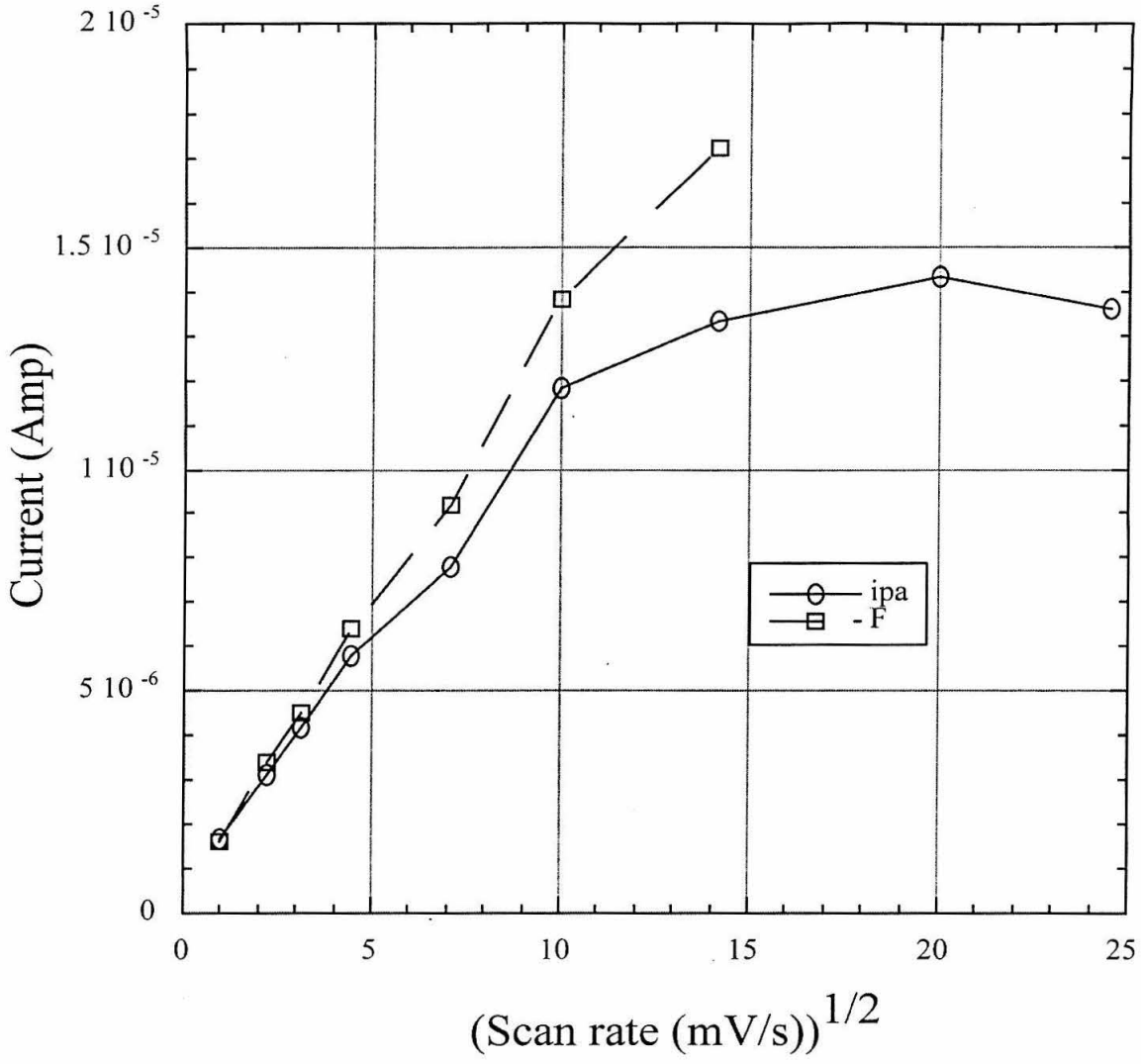
2 10 -5
1.5 10 -5
1 10 -5
5 10 -6
0
Current (Amp)
0
5
10
15
20
25
(Scan rate (mV/s))1/2
ipa
- F

Figure 2.12: EPR spectrum of P94F and wild type amicyanin.

EPR of Amicyanin

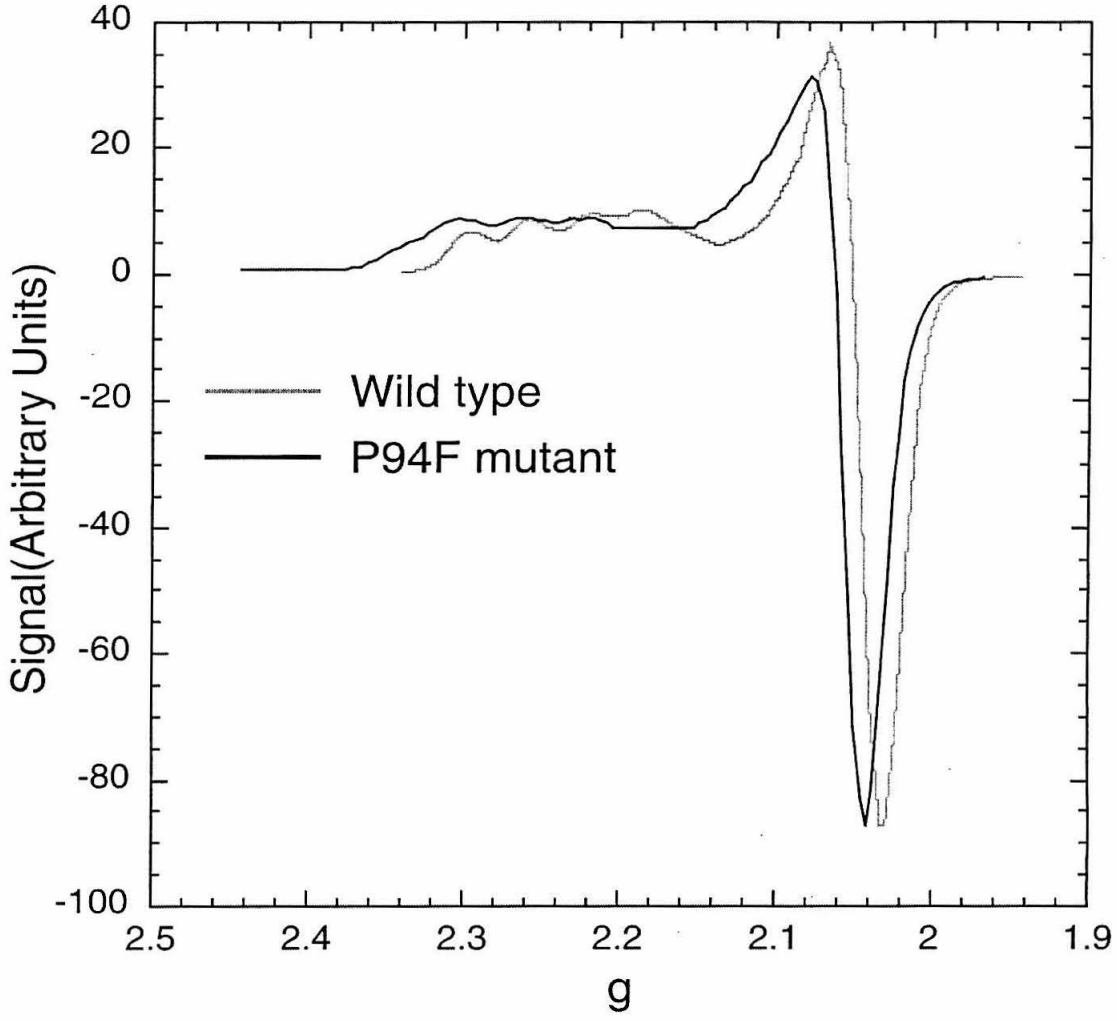

	Wild type	P94F
$g_{\|\|}$	2.2428	2.2369
$A_{\|\|}$	7.4×10^{-3} cm^{-1}	9.45×10^{-3} cm^{-1}
$g_{\perp}$	2.0481	2.0603

Figure 2.13: X-ray structure of poplar plastocyanin's active site, detailing the docking of the protonated histidine ligand to the proline carbonyl. The sphere in the center is the Cu^{1+} ion, bound in a trigonal plane by His-Cys-Met ligation. Dashed lines indicate hydrogen bonds.

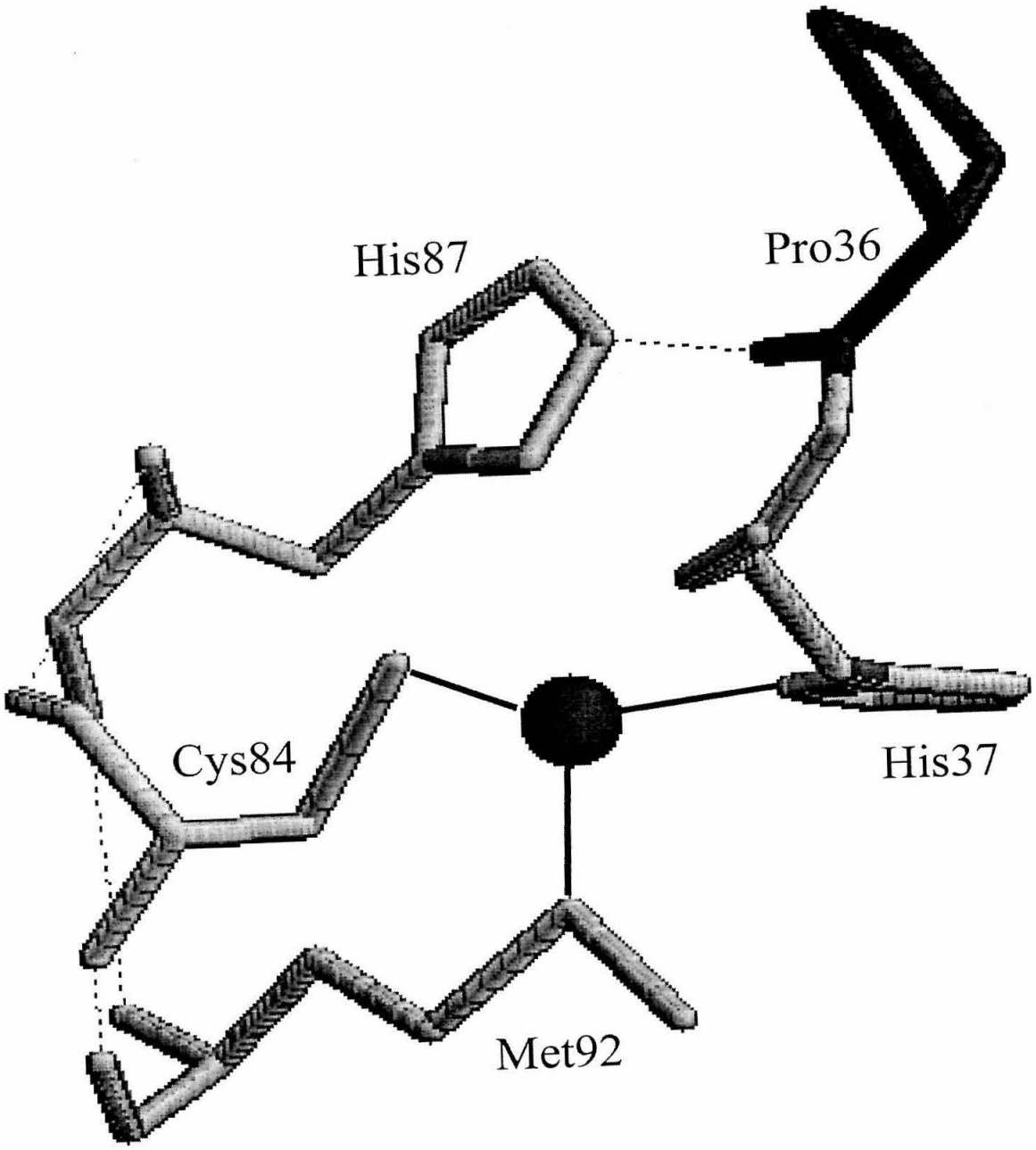
His87
Pro36
Cys84
His37
Met92

Figure 2.14: Electrochemistry of P52G, (M28,51F), and (M28,51F,P52G) mutants.

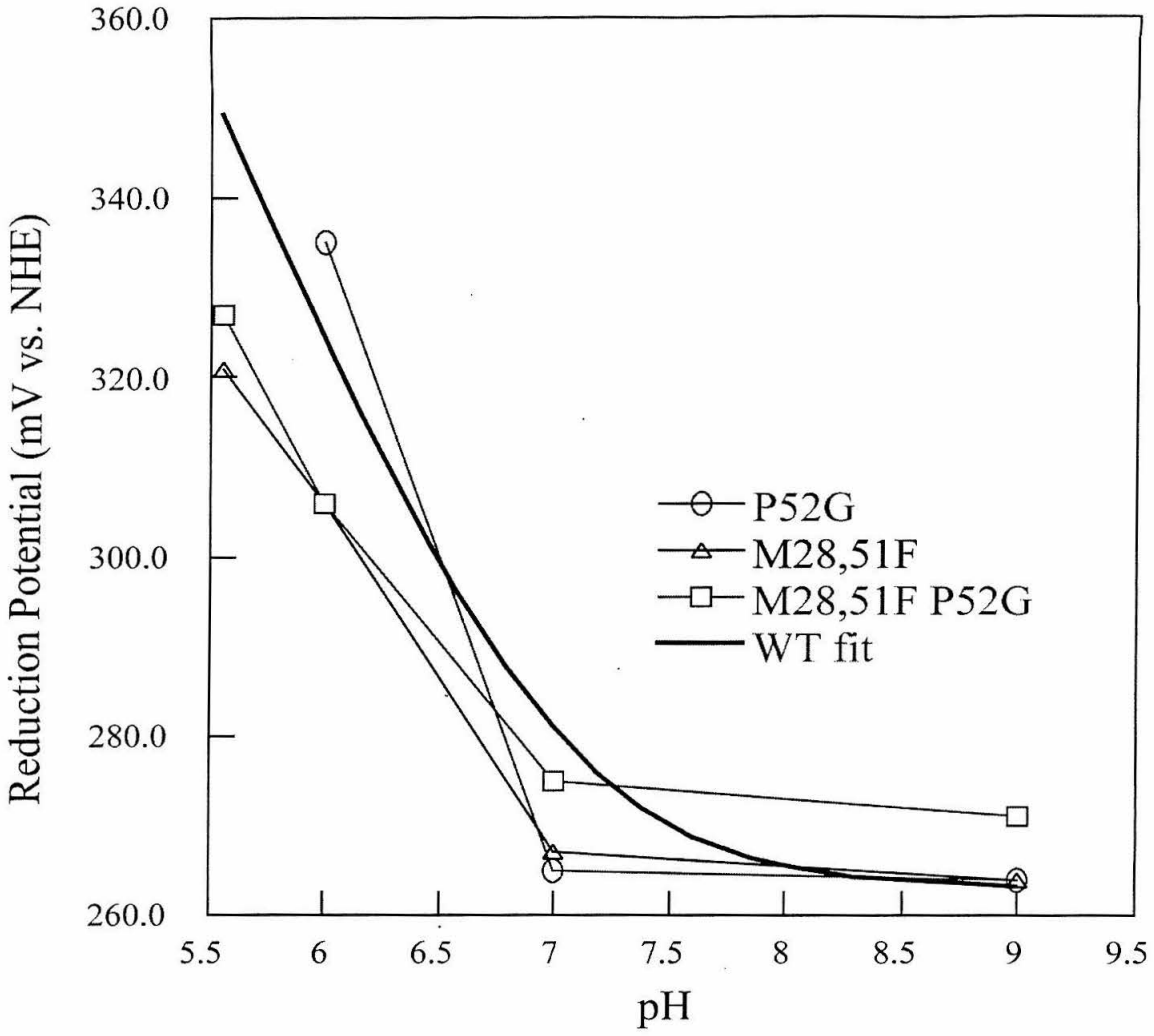
360.0
340.0
320.0
300.0
280.0
260.0
Reduction Potential (mV vs. NHE)
5.5
6
6.5
7
7.5
8
8.5
9
9.5
pH
P52G
M28,51F
M28,51F P52G
WT fit

1)Guss, J. M.; Harrowell, P. R.; Murata, M.; Norris, V. A.; Freeman, H. C. *J. Mol. Biol.* **1986**, *192*, 361-387.

2)Vakoufari, E.; Wilson, K. S.; Petratos, K. *FEBS Letters* **1994**, *347*, 203-206.

3)Lommen, A.; Canters, G. W. *J. Biol. Chem.* **1990**, *265*, 2768-2774.

4)Battistuzzi, G.; Borsari, M.; Loschi, L.; Sola, M. *JBIC* **1997**, *2*, 350-359.

5)St. Clair, C. S.; Ellis, W. R.; Gray, H. B. *Inorg. Chim. Acta* **1992**, *191*, 149-155.

6)Zhu, Z. Y.; Cunane, L. M.; Chen, Z. W.; Durley, R. C. E.; Mathews, F. S.; Davidson, V. L. *Biochemistry* **1998**, *37*, 17128-17136.

7)Katoh, S. *Nature (London)* **1960**, *186*, 533-534.

8)Katoh, S.; Shiratori, I.; Takamiya, A. *J. Biochem. (Tokyo)* **1962**, *51*, 32-40.

9)Brill, A. S.; Martin, R. B.; Williams, R. J. P. ; Pullman, B., Ed.; Academic: New York, 1964.

10)Markley, J. L.; Ulrich, E. L.; Berg, S. P.; Krogmann, D. W. *Biochemistry* **1975**, *14*, 4428-4433.

11)Colman, P. M.; Freeman, H. C.; Guss, J. M.; Murata, M.; Norris, V. A.; Ramshaw, J. A. M.; Venkatappa, M. P. *Nature* **1978**, *272*, 319-324.

12)Sinclair-Day, J. D.; Sisley, M. J.; Sykes, A. G.; King, G. C.; Wright, P. E. *J. Chem. Soc. Chem. Commun.* **1985**, *8*, 505-507.

13)Dennison, C.; Kohzuma, T.; McFarlane, W.; Suzuki, S.; Sykes, A. G. *J. Chem. Soc. Chem. Comm.* **1994**, *5*, 581-582.

14)Sykes, A. G. *Struct. Bond.* **1991**, *75*, 175-224.

15)Guss, J. M.; Merritt, E. A.; Phizackerley, R. P.; Freeman, H. C. *J. Mol. Biol.* **1996**, *262*, 686-705.

16)Nishiyama, M.; Suzuki, J.; Ohnuki, T.; Chang, H. C.; Horinouchi, S.; Turley, S.; Adman, E. T.; Beppu, T. *Prot. Eng.* **1992**, *5*, 177-184.

17)Libeu, C. A. P.; Kukimoto, M.; Nishiyama, M.; Horinuchi, S.; Adman, E. T. *Biochemistry* **1997**, *36*, 13160-13179.

18)Husain, M.; Davidson, V. L. *J. Biol. Chem.* **1985**, *260*, 14626-14629.

19)Cunane, L. M.; Chen, Z. W.; Durley, R. C. E.; Mathews, F. S. *Acta. Cryst. D* **1996**, *52*, 676-686.

20)Davidson, V. L.; Jones, L. H. *Biochemistry* **1996**, *35*, 8120-8125.

21)Chen, L.; Durley, R. C. E.; Mathews, F. S.; Davidson, V. L. *Science* **1994**, *264*, 86-90.

22)Chen, L. Y.; Durley, R.; Poliks, B. J.; Hamada, K.; Chen, Z. W.; Mathews, F. S.; Davidson, V. L.; Satow, Y.; Huizinga, E.; Vellieux, F. M. D.; Hol, W. G. J. *Biochemistry* **1992**, *31*, 4959-4964.

23)Davidson, V. L.; Joens, L. H. *J. Biol. Chem.* **1995**, *270*, 23941-23943.

24)O'Reilly, J. E. *Biochim. Biophys. Acta* **1973**, *292*, 509-515.

25)Janz, G. J. *Silver-Silver Halide Electrodes*; Ives, D. J. G. and Janz, G. J., Ed.; Academic: New York, 1961.

26)Bard, A. J.; Faulkner, L. R. *Electrochemical Methods*; John Wiley and Sons: New York, 1980.

27)Nowinski, S. A.; Anjo, D. M. *J. Chem. Eng. Data* **1989**, *34*, 265-268.

28)Conrad, L. S.; Hill, H. A. O.; Hunt, N. I.; Ulstrup, J. *J. Electroanal. Chem.* **1994**, *264*, 17-22.

29)Armstrong, F. A.; Hill, H. A. O.; Oliver, B. N.; Whitford, D. *J. Am. Chem. Soc.* **1985**, *107*, 1473-1476.

30)Sakurai, T.; Nose, F.; Fujiki, T.; Suzuki, S. *Bull. Chem. Soc. Jpn.* **1996**, *69*.

31)Kohzuma, T.; Dennison, C.; McFarlane, W.; Nakashima, S.; Kitagawa, T.; Inoue, T.; Kai, Y.; Nishio, N.; Shidara, S.; Suzuki, S.; Sykes, A. G. *J. Biol. Chem.* **1995**, *270*, 25733-25738.

32)Clark, W. M. *Oxidation-Reduction Potentials of Organic Systems*; Williams and Wilkins: Baltimore, 1960.

33)Inoue, T.; Gotowda, M.; Sugawara, H.; Kohzuma, T.; Yoshizaki, F.; Sugimura, Y.; Kai, Y. *Biochemistry* **1999**, *38*, 13853-13861.

34)Kohzuma, T.; Inoue, T.; Yoshizaki, F.; Sasakawa, Y.; Onodera, K.; Nagatomo, S.; Kitagawa, T.; Uzawa, S.; Isobe, Y.; Sugimura, Y.; Gotowda, M.; Kai, Y. *J. Biol. Chem.* **1999**, *274*, 11817-11823.

35)Baker, E. N. *J. Mol. Biol.* **1988**, *203*, 1071-1095.

36)Nar, H.; Messerschmidt, A.; Huber, R.; van de Kamp, M.; Canters, G. W. *J. Mol. Biol.* **1991**, *221*, 765-772.

37)Botuyan, M. V.; Toy-Palmer, A.; Chung, J.; Blake II, R. C.; Beroza, P.; Case, D. A.; Dyson, H. C. *J. Mol. Biol.* **1996**, *263*, 752-767.

38)Sigfridsson, K.; Young, S.; Hansson, Ö. *Eur. J. Biochem.* **1997**, *245*, 805-812.

39)Wittung-Stafshede, P.; Gomez, E.; Öhman, A.; Aasa, R.; Villahermosa, R. M.; Leckner, J.; Karlsson, B. G.; Sanders, D.; Fee, J. A.; Winkler, J. R.; Malmström, B. G.; Gray, H. B.; Hill, M. G. *Biochem. Biophys. Acta* **1998**, *1388*, 437-443.

40)Hoitink, C. W. G.; Canters, G. W. *J. Biol. Chem.* **1992**, *267*, 13836-13842.

Chapter 3:

Thermal Denaturation of Amicyanin

Temperature-dependent Research:

Work reported in Chapter two has shown that the presence of the second hydrogen bond to the cysteine thiolate increased the strength of the rack. However, one of the goals was to quantify the rack, which may be accomplished by measuring the shift in the pK_a of the imidazole in the copper(I) state. Amicyanin, the protein with the highest pK_a, was chosen because it should allow the largest pH "window" for the observation of change. Unfortunately, low pH measurements are challenging and sometimes impossible to make; protein stability and electrode interactions became difficulties near pH 5.0, which is not surprising since the pI of amicyanin is 4.8.

Another way to measure stability is to unfold the protein by increasing the temperature[1]. Protein structure was monitored primarily by circular dichroism in the far ultraviolet (210-250 nm). Measurements were made at pH 6.0 and ph 8.0, effectively bracketing the pK_a of His95 in reduced, wild type amicyanin; at one pH, 90% of His95 is protonated, contrary to the other pH where 90% is fully ligated. By choosing a small pH spread, stability effects due to other protonation events are minimized. The metal was removed from the protein to distinguish phenomena occurring at the metal site from those occurring elsewhere in the protein.

Materials and Methods:

Preparation of Apoamicyanin: 3mLs of approximately 100 μM amicyanin was placed in 10 mM TRIS at pH 8.0 with an excess of dithionite and 0.1 M KCN. After 20 hours, the sample was exchanged into fresh 10 mM TRIS pH 8.0.

Circular dichroism spectroscopy: All measurements were carried out on a (spectrometer name) spectrometer in a 1.000 cm pathlength cell. Protein concentrations were typically 5-10 μM. Wavelength scans spanned from 250 – 210 nm, integrating at each wavelength (one nm steps) for five seconds with a 1.5 nm bandwidth. Temperature scans were typically from 298 to 358 K in two-degree intervals. Reversed scans were initiated immediately after the forward scans.

Results and Discussion:

The circular dichroism spectrum at room temperature is characteristic of a twisted interacting β-sheet[2]. The ellipticity at 220 nm as the temperature is varied clearly demonstrates three states: a native (N), an intermediate (I), and an unfolded form (U). The transition from N to I involves a decrease in the magnitude of ellipticity, while the transition from I to U (or N to U) involves an increase. Table 3.1 condenses the information found in the melting curves in Figures 3.1-3.6. Each of these figures also features the spectra taken before and after the melting curves were performed.

These data indicate some trends. As Luo demonstrated in his thesis[3], the removal of metal destabilizes the overall fold of the protein, as the melting temperature for the unfolded *P. aeruginosa* azurin drops approximately 15 degrees. The assignment of the U state to a large scale unfolding of the protein seems reasonable in that the P94F mutation doesn't affect the relevant melting temperature.

Table 3.1: Melting curve parameters for amicyanin.

Mutation	Redox State	pH	T_m (I state)	T_m (U state)	Comments
Wild Type	Red	8.0	46	69	
Wild Type	Ox	8.0	47	70	
Wild Type	Red	6.0	58	70	
Wild Type	Ox	6.0	57	75	
P94F	Red	8.0	44	73	
P94F	Ox	8.0	44	?	V. small I state
P94F	Red	6.0	44	60?	
P94F	Ox	6.0	-	74	U is ppt.
Apo WT	N/A	8.0	-	54	U is shallow
Apo WT	N/A	6.0	-	54	U is sharp
Apo P94F	N/A	8.0	-	55	Shallow
Apo P94F	N/A	6.0	-	62	

The high temperature for thermal unfolding often exceeds 70 degrees C, and has been ascribed to a number of factors in different blue copper proteins, including intramolecular hydrogen bonds, hydrophobic effects, stabilization by copper ion binding, and disulfide bridges (which amicyanin does not possess)[4-7]. Plastocyanin is quickly degraded without the presence of copper in the medium[8].

The presence of the I state, on the other hand, seems directly related to the metal site because the apo-enzymes lack this melting phase. An explanation could be that the I state becomes destabilized so that it is now observed at room temperature. However, the ratio of the CD signal at 220 nm to the absorption at 280 nm is the same for the apo-form as for the wild type, suggesting that they share the native structure. Another possibility is that the I state is destabilized, but many other states that display native-like CD signals are also present at room temperature. A third explanation is that the I state is stabilized above the U state, which implies that the presence of copper stabilizes the metal-binding

site[7,9]. Essentially, a combination of the mutation and copper(II) structural preferences could make the I state very high in energy.

There are other possibilities. So far, discussion of the state characterizations has occurred from a native-centric view, as if the stabilities of the native states are unaffected by mutation, oxidation/reduction, or pH changes. In fact, since dramatic changes have occurred in the reduction potential and structure because of mutation, redox state, and pH, it is just as likely that the stabilities of the native structures are changing. Since only differences in free energy may be measured, it is difficult to tell to what extent each state is changing. The I⇔U melting temperatures are very similar to each other over a range of pHs and both redox states in the wild type. It is unlikely that the N and U states change by the same amount; it is tempting to say, then, that the N state energetics are constant because the N⇔U temperature gap is constant. [This assumption would be a grievous error.]

The free energy of thermal unfolding is described by the modified Gibbs-Helmholtz equation[1] (1):

$$\Delta G(T) = \Delta H_m\left(1 - \frac{T}{T_m}\right) - \Delta C_p\left[\left(T_m - T\right) + T\ln\left(T/T_m\right)\right] \qquad (1)$$

where ΔG and ΔH are the Gibbs free energy and enthalpy, ΔC_p is the change in the isobaric heat capacity, T is the temperature, and T_m is the melting temperature. The first difficulty with assigning values for energy to the melting curves is that the heat capacity

change, ΔC_p, has not been measured for the melting process. This parameter is usually measured by differential scanning calorimetry. This equation also shows that the melting temperature, T_m, is an empirical parameter indicating the temperature at which half of the transition has been completed. Thus, it is unfortunately not linked to any of the desired thermodynamic parameters except that it sets an assigned value for one point on the curve. Different melting temperatures indicate different thermal stabilities, but not different state to state free energy gaps, which would be obtained by fitting the shape of the melting transition.

The melting temperature of the I state appears to be pH-dependent in the wild type, but pH-independent in the P94F mutant, similar to the reduction potential in the last chapter. In addition, while the melting temperature has no dependence on the redox state of the metal in either the wild type or the mutant, intensity of the phase change is nearly zero in the oxidized form of P94F! The phase change in reduced P94F is similar to that in either wild type transition, but only half as intense with a less sharp transition. The CD spectrum of oxidized P94F at 50 degrees centigrade is identical with the spectrum at room temperature (Figure 3.7); therefore, little structural change, if any, is occurring in this sample. The N$\Leftrightarrow$I transition was found to be fully reversible in wild type protein at pH 8.0, but irreversible at pH 6.0 (Figures 3.8-3.9). This transition in the P94F mutant was irreversible at both pHs, but lost more structure at pH 6 than at pH 8 (Figure 3.10). This result indicates that the I state may involve a protonatable group with a pK_a between 8 and 6, possibly the C-terminal histidine ligand. Also, the hydrogen bond or packing forces of the phenylalanine may restrict the copper site from accessing the I state. Once

that bond or packing is disrupted, return to the native state is improbable. Similar pH dependences in plastocyanin are thought to involve a surface tyrosine[10].

Specifically, what part of the protein is changed in the N⇔I transition? To answer this question, several studies were performed. Spectroscopies sensitive to different regions of the protein were used to probe the I state. The absorbance of each of the blue copper bands was observed to be independent of temperature until the onset of the U state. The aromatic region (260-300 nm) showed a slight (20%) irreversible increase in absorbance. However, no change was witnessed in the CD of the aromatic region. In addition, EPR spectroscopic measurements were made on a sample of wild type amicyanin that had been flash frozen from 55 degrees centigrade (Figure 3.11). The spectrum is identical with a sample frozen from room temperature. Taken together, these results suggest that the oxidized copper maintains its geometry[11], but possibly the surrounding region is affected.

In previous experiments with GdnHCl, it was found that there is a slightly unfolded form of azurin assigned to a "loosening" of the surrounding structure[12]. This loosening allowed the reduced form of the protein to rearrange into a less restricted form; this rearrangement was experimentally observed as an increase in the reduction potential. The reduction potentials of the wild type and P94F amicyanins were measured at temperatures ranging from 25 to 55 degrees centigrade (at which point the edge plane-graphite electrode was unresponsive to any samples or standards). Potentials increased linearly with temperature, with no abrupt changes that would correspond to the

chaotropically loosened state. Equations 2 and 3 were used to calculate the enthalpy and entropy of reduction. F is Faraday's constant, n is the number of electrons transferred, T is the temperature, and E_m is the midpoint potential of the cyclic voltammogram. The enthalpy of reduction was measured to be ~ –41 kJ/mol in both the wild type and the mutant by plotting E_m/T vs. 1/T (Figures 3.12-3.13). The entropy of reduction varied from –53.3 J/mol K in the wild type to –8.6 J/mol K in P94F, both of which are within the range of blue copper proteins[13-15] (Table 3.2).

$$\Delta G = -nFE_m \qquad (2)$$

$$\frac{\Delta G}{T} = \frac{\Delta H}{T} - \Delta S \qquad (3)$$

Entropy differences in these proteins are ascribed to solvent rearrangements. The side of the C-terminal histidine ligand opposite the copper is normally hydrogen bound to a water network[16-19], so this change in entropy could be due to a tightening of the loop structure that draws the histidine into the protein, as one would expect from the proposed mutant hydrogen bond. 43 J/mol K is a large difference in entropy. The removal of a single water molecule from a strong acceptor, such as a metal ion, has been estimated to be 29 J/mol K[20]; however, the blue copper proteins alone span a range from 31 to -58 J/mol K, indicating that there is something fundamental to the protein structure that may account for this large a change.

Table 3.2: Enthalpies, entropies, and potentials of reduction.

Protein/Compound	ΔH (kJ/mol)	ΔS (J/mol K)	$E^{0'}$ (mV vs. NHE)
WT Amicyanin	-40.9	-53.3	260 (pH 8.0)
P94F Amicyanin	-41.6	-8.6	410
Plastocyanin (*S. oleracea*)	-46	-36	366
Plastocyanin (*P. Vulgaris*)	-38	-10	360
Plastocyanin (*C. sativus*)	-45	-30	374
Azurin (*P. aeruginosa*)	-49	-65	307
Azurin (*A. denitrificans*)	-36	-32	276
Azurin (*A. faecalis*)	-43	-58	266
Stellacyanin (*R. vernicifera*)	-25	-22	187
Stellacyanin (*C sativus*)	-32	-21	265
CBP (*C. sativus*)	-20	+31	306
SBP (*S. oleracea*)	-31	+7	345
Umecyanin (*A. laphatifolia*)	-33	-17	290
Fungal laccase (*P. versicolor*)	-73.1	+7.1	780
Rubredoxin (*C. pasteurianum*)	-41.8	-150.6	-55
Rubredoxin (*P. furiosus*)	-54.4	-171.5	31
$Ru(bpy)_3^{+/0}$ (acetonitrile)		25	

Comparisons between the mutant and wild type melting curves indicate that the additional hydrogen bond (or phenyl ring) restricts the I state from fully forming. The

only example of an unfolding feature in blue copper proteins occurring at such a low temperature has been found by Muga and coworkers[21]. They have measured the FTIR spectra of the amide I bands of poplar plastocyanin as a function of temperature. Specifically, there is an increase in intensity of a component at 1665 cm^{-1} as the temperature reaches 40 degrees centigrade. They did not assign this change, but did assign overall melting temperatures between 45 and 53 degrees centigrade at pH 4.8. This transition temperature increases between 13 and 20 degrees with a pH increase of 2.2 units, a similar magnitude but opposite direction as found in the I state.

Summary:

The melting of amicyanin has been identified as a three-state process, involving a thermodynamic intermediate with pH-dependent reversibility that is linked to the metal site by investigations of apoamicyanin. Comparisons of the wild type and P94F mutant show that the additional hydrogen bond has the effect of reducing the magnitude of change between the native and intermediate states. The melting temperature of the intermediate state in the mutant is pH-independent; however, the melting temperature of the wild type increases with decreasing pH, indicating that the region near the metal site becomes more stable in the wild type.

As shown in Chapter two, this is the opposite of the case for the metal-ligand interactions, where it is the mutation that makes the copper-histidine bond more resistant to dissociation. These two results show that the mutation stabilizes a local interaction, i.e., the metal-ligand bonding, at a cost to the nearby protein matrix. The original idea of

global energetics being used to stabilize a high-energy configuration is supported by these findings.

Figure 3.1: Melting curves of reduced wild type amicyanin at pH 8.0 and pH 6.0. The forward melt, taken while increasing the temperature, is represented by a solid line; the reverse melt, taken while decreasing the temperature, is represented by a dashed line. Inset: Full CD curves taken before and after the melt/reverse melt process at 25 degrees C. Protein at the beginning of the experiment is represented by the solid curves, while protein after the experiment is represented by the dashed curves.

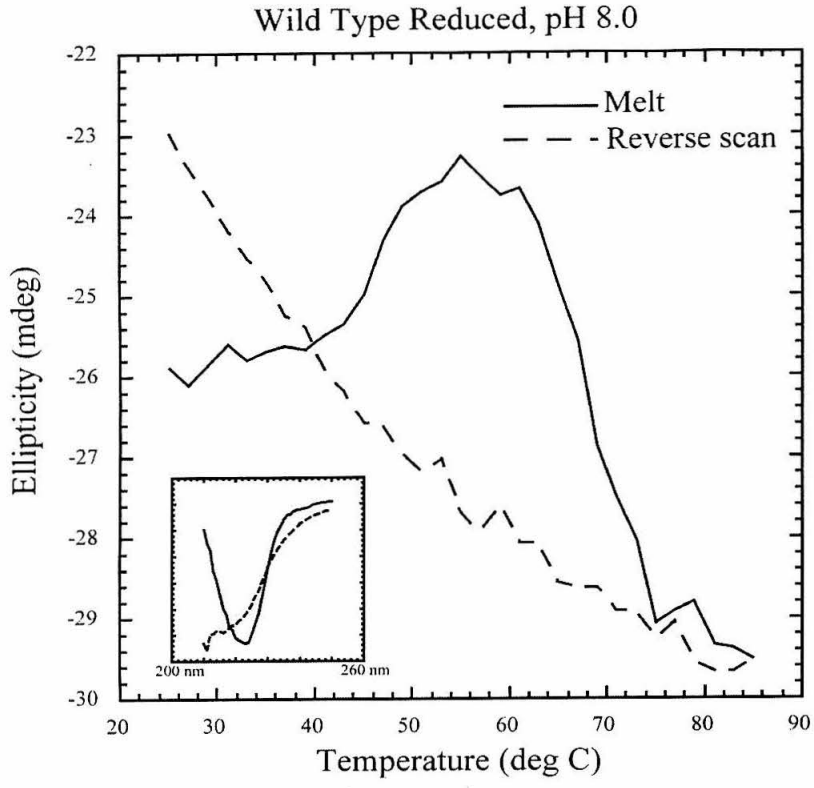
Wild Type Reduced, pH 8.0
Melt
Reverse scan
Ellipticity (mdeg)
Temperature (deg C)
200 nm
260 nm

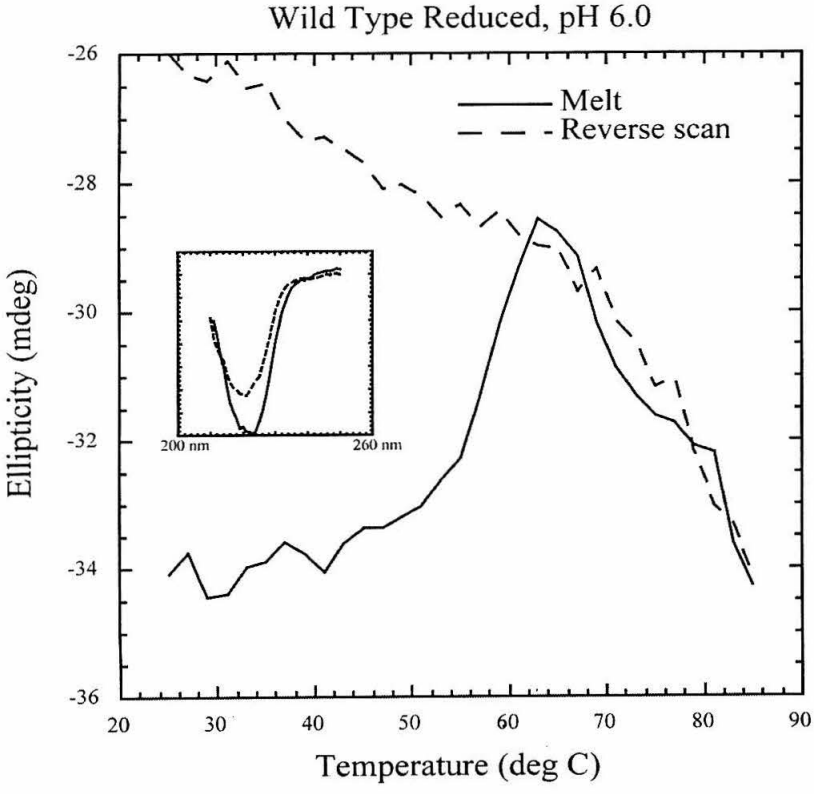
Wild Type Reduced, pH 6.0
Melt
Reverse scan
Ellipticity (mdeg)
Temperature (deg C)
200 nm
260 nm

Figure 3.2: Melting curves of oxidized wild type amicyanin at pH 8.0 and pH 6.0. The forward melt, taken while increasing the temperature, is represented by a solid line; the reverse melt, taken while decreasing the temperature, is represented by a dashed line. Inset: Full CD curves taken before and after the melt/reverse melt process at 25 degrees C. Protein at the beginning of the experiment is represented by the solid curves, while protein after the experiment is represented by the dashed curves.

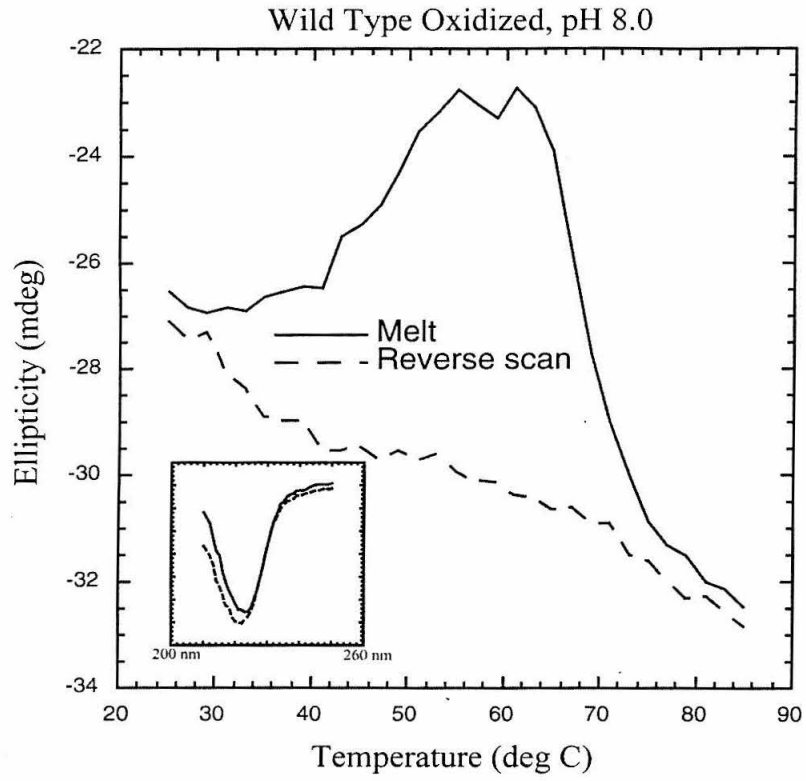
Wild Type Oxidized, pH 8.0
Ellipticity (mdeg)
Temperature (deg C)
Melt
Reverse scan
200 nm
260 nm
-22
-24
-26
-28
-30
-32
-34
20
30
40
50
60
70
80
90

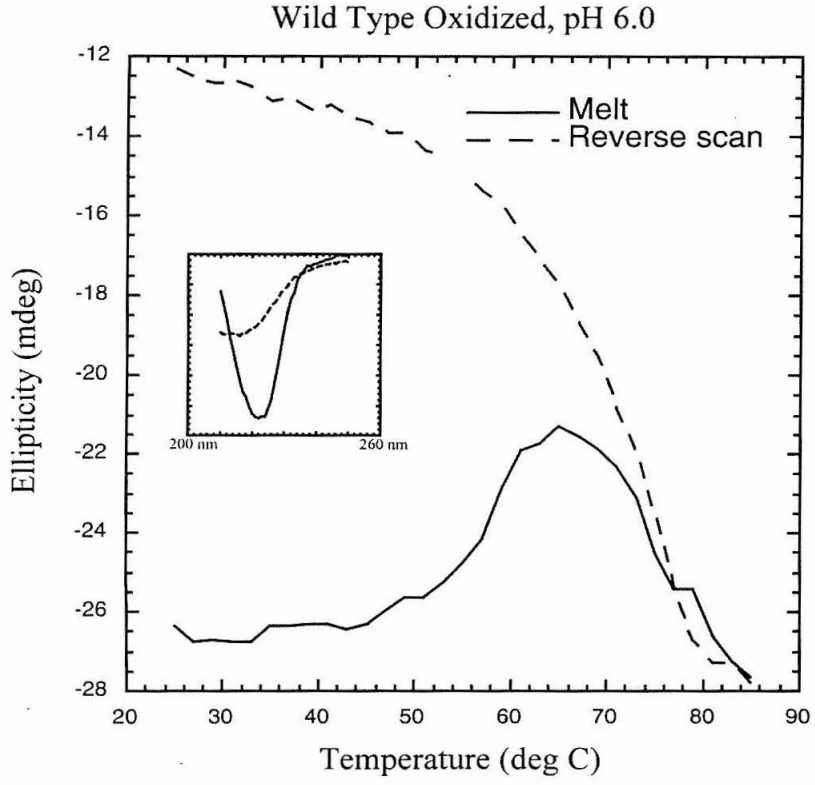
Wild Type Oxidized, pH 6.0
Ellipticity (mdeg)
Temperature (deg C)
Melt
Reverse scan
200 nm
260 nm
-12
-14
-16
-18
-20
-22
-24
-26
-28
20
30
40
50
60
70
80
90

Figure 3.3: Melting curves of reduced P94F amicyanin at pH 8.0 and pH 6.0. The forward melt, taken while increasing the temperature, is represented by a solid line; the reverse melt, taken while decreasing the temperature, is represented by a dashed line. Inset: Full CD curves taken before and after the melt/reverse melt process at 25 degrees C. Protein at the beginning of the experiment is represented by the solid curves, while protein after the experiment is represented by the dashed curves.

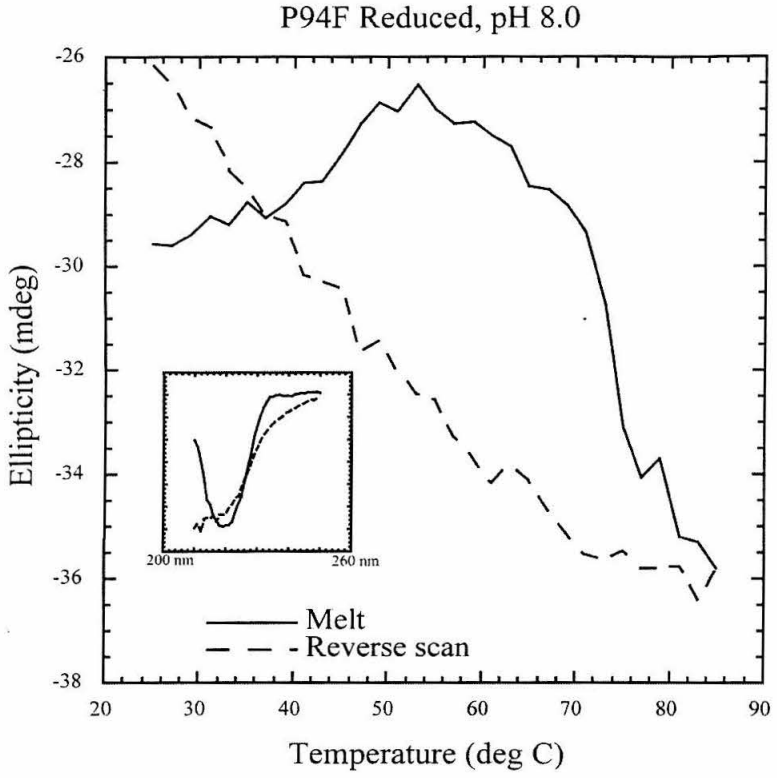
P94F Reduced, pH 8.0
Ellipticity (mdeg)
-26
-28
-30
-32
-34
-36
-38
20
30
40
50
60
70
80
90
Temperature (deg C)
200 nm
260 nm
Melt
Reverse scan

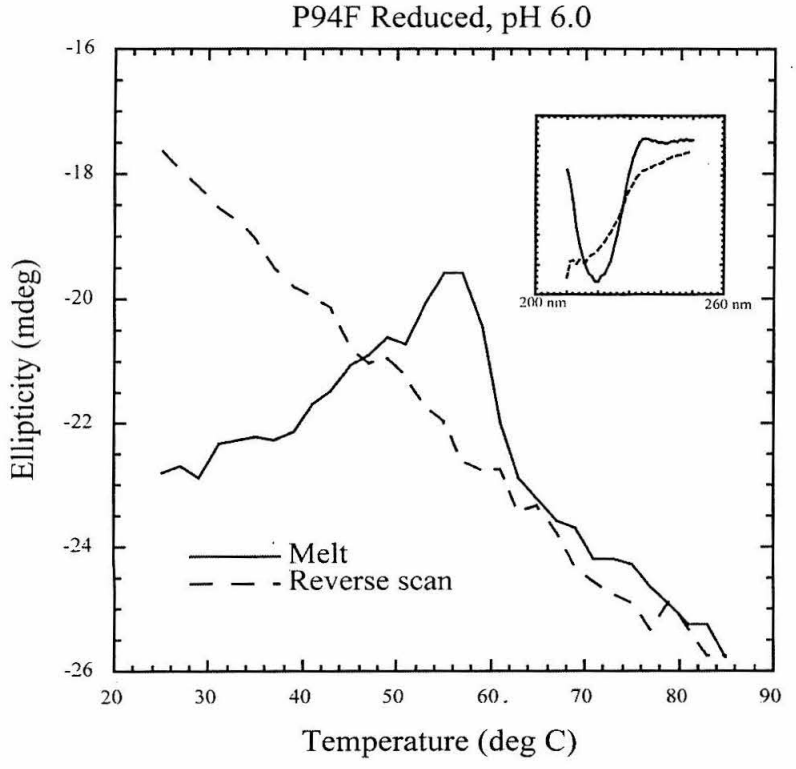
P94F Reduced, pH 6.0
Ellipticity (mdeg)
-16
-18
-20
-22
-24
-26
20
30
40
50
60
70
80
90
Temperature (deg C)
200 nm
260 nm
Melt
Reverse scan

Figure 3.4: Melting curves of oxidized P94F amicyanin at pH 8.0 and pH 6.0. The forward melt, taken while increasing the temperature, is represented by a solid line; the reverse melt, taken while decreasing the temperature, is represented by a dashed line. Inset: Full CD curves taken before and after the melt/reverse melt process at 25 degrees C. Protein at the beginning of the experiment is represented by the solid curves, while protein after the experiment is represented by the dashed curves.

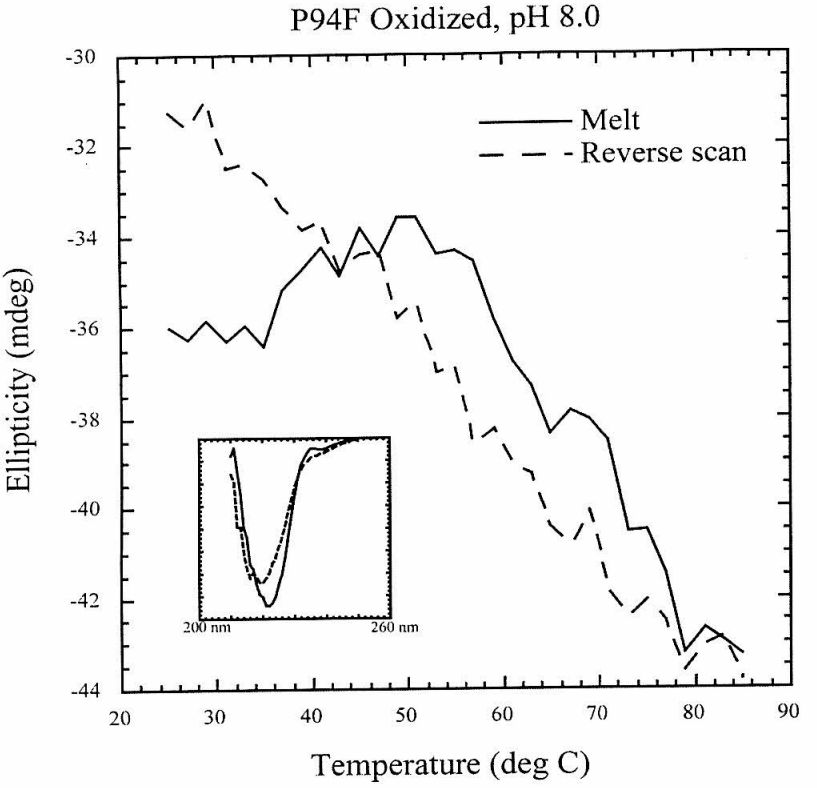
P94F Oxidized, pH 8.0
Melt
Reverse scan
Ellipticity (mdeg)
Temperature (deg C)
200 nm
260 nm

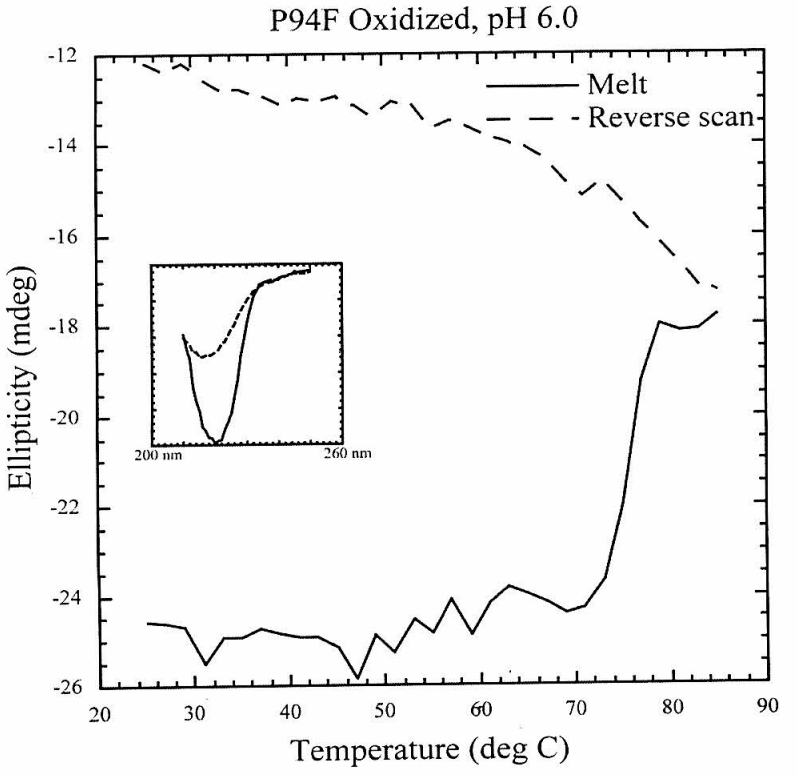
P94F Oxidized, pH 6.0
Melt
Reverse scan
Ellipticity (mdeg)
Temperature (deg C)
200 nm
260 nm

Figure 3.5: Melting curves of wild type apoamicyanin at pH 8.0 and pH 6.0. The forward melt, taken while increasing the temperature, is represented by a solid line; the reverse melt, taken while decreasing the temperature, is represented by a dashed line. Inset: Full CD curves taken before and after the melt/reverse melt process at 25 degrees C. Protein at the beginning of the experiment is represented by the solid curves, while protein after the experiment is represented by the dashed curves.

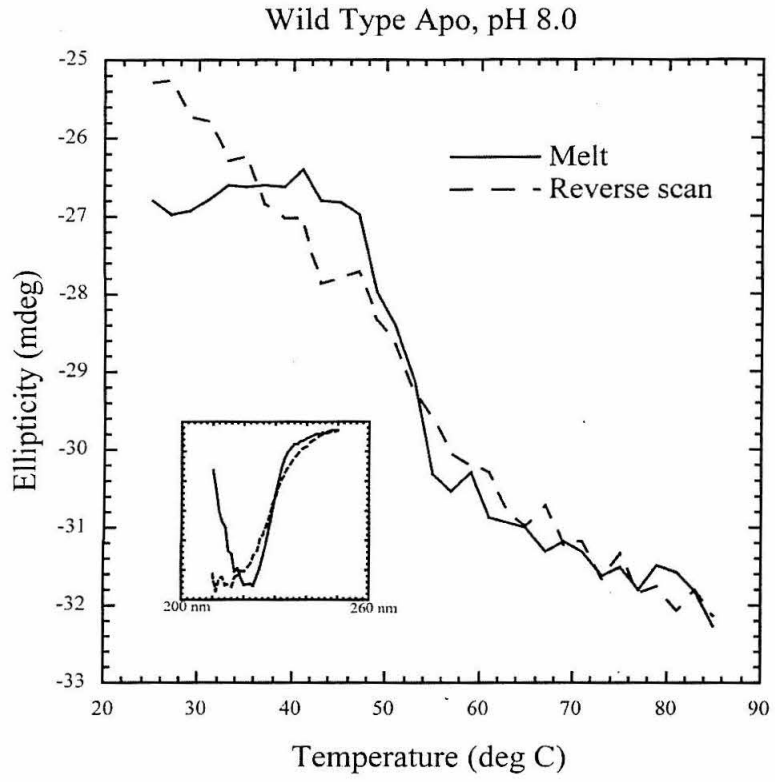
Wild Type Apo, pH 8.0
Ellipticity (mdeg)
Temperature (deg C)
Melt
Reverse scan
200 nm
260 nm

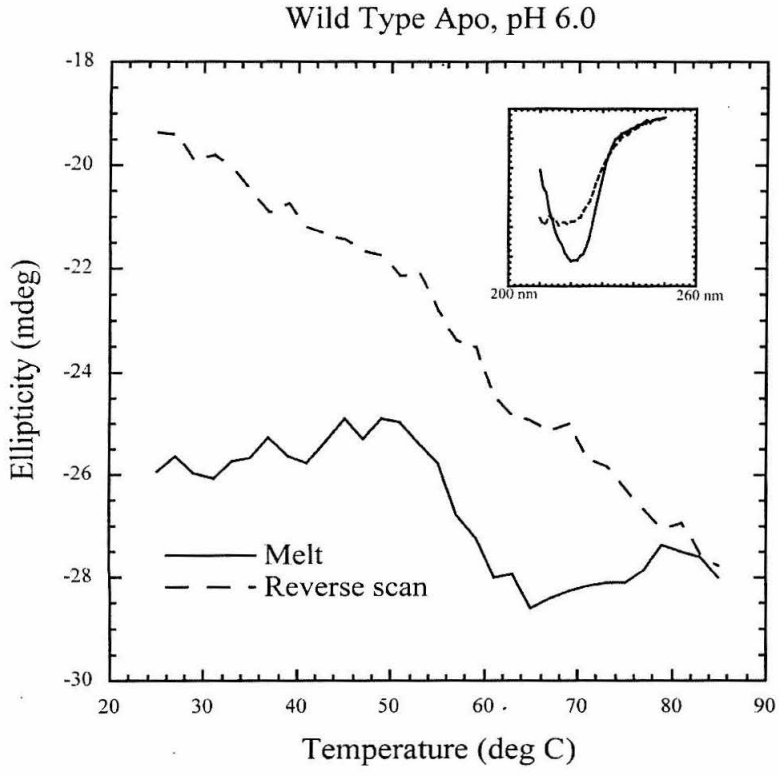
Wild Type Apo, pH 6.0
Ellipticity (mdeg)
Temperature (deg C)
Melt
Reverse scan
200 nm
260 nm

Figure 3.6: Melting curves of P94F apoamicyanin at pH 8.0 and pH 6.0. The forward melt, taken while increasing the temperature, is represented by a solid line; the reverse melt, taken while decreasing the temperature, is represented by a dashed line. Inset: Full CD curves taken before and after the melt/reverse melt process at 25 degrees C. Protein at the beginning of the experiment is represented by the solid curves, while protein after the experiment is represented by the dashed curves.

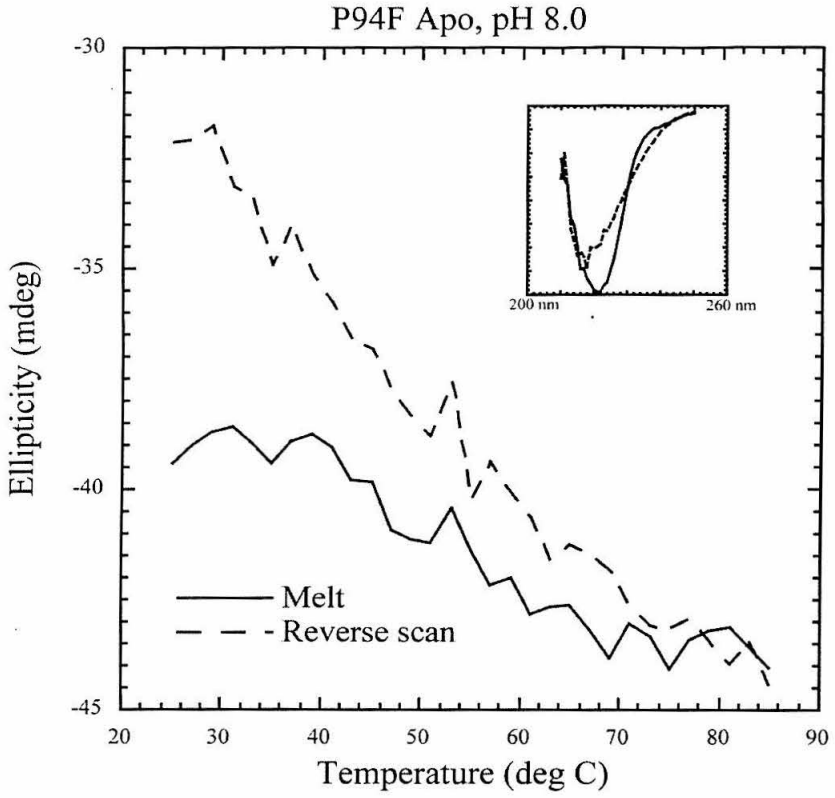
P94F Apo, pH 8.0
Ellipticity (mdeg)
-30
-35
-40
-45
20
30
40
50
60
70
80
90
Temperature (deg C)
Melt
Reverse scan
200 nm
260 nm

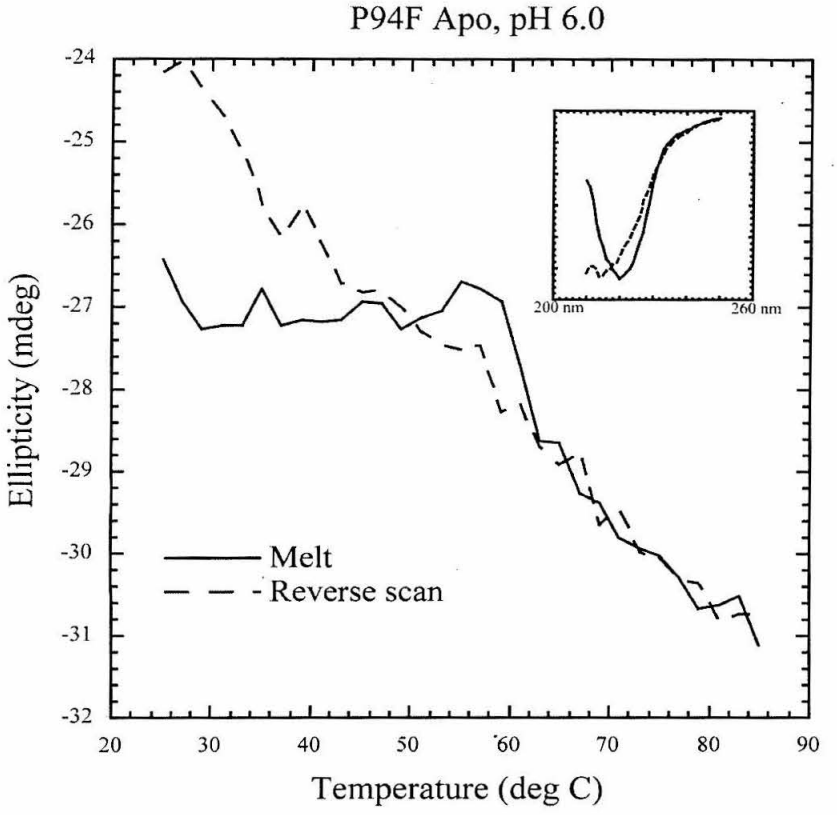
P94F Apo, pH 6.0
Ellipticity (mdeg)
-24
-25
-26
-27
-28
-29
-30
-31
-32
20
30
40
50
60
70
80
90
Temperature (deg C)
Melt
Reverse scan
200 nm
260 nm

Figure 3.7: UV circular dichroism spectra of oxidized P94F at pH 8.0. Solid line represents spectrum taken at 25 degrees C, dashed line represents spectra taken at 55 degrees C. Similarity indicates no major structural differences at these temperatures.

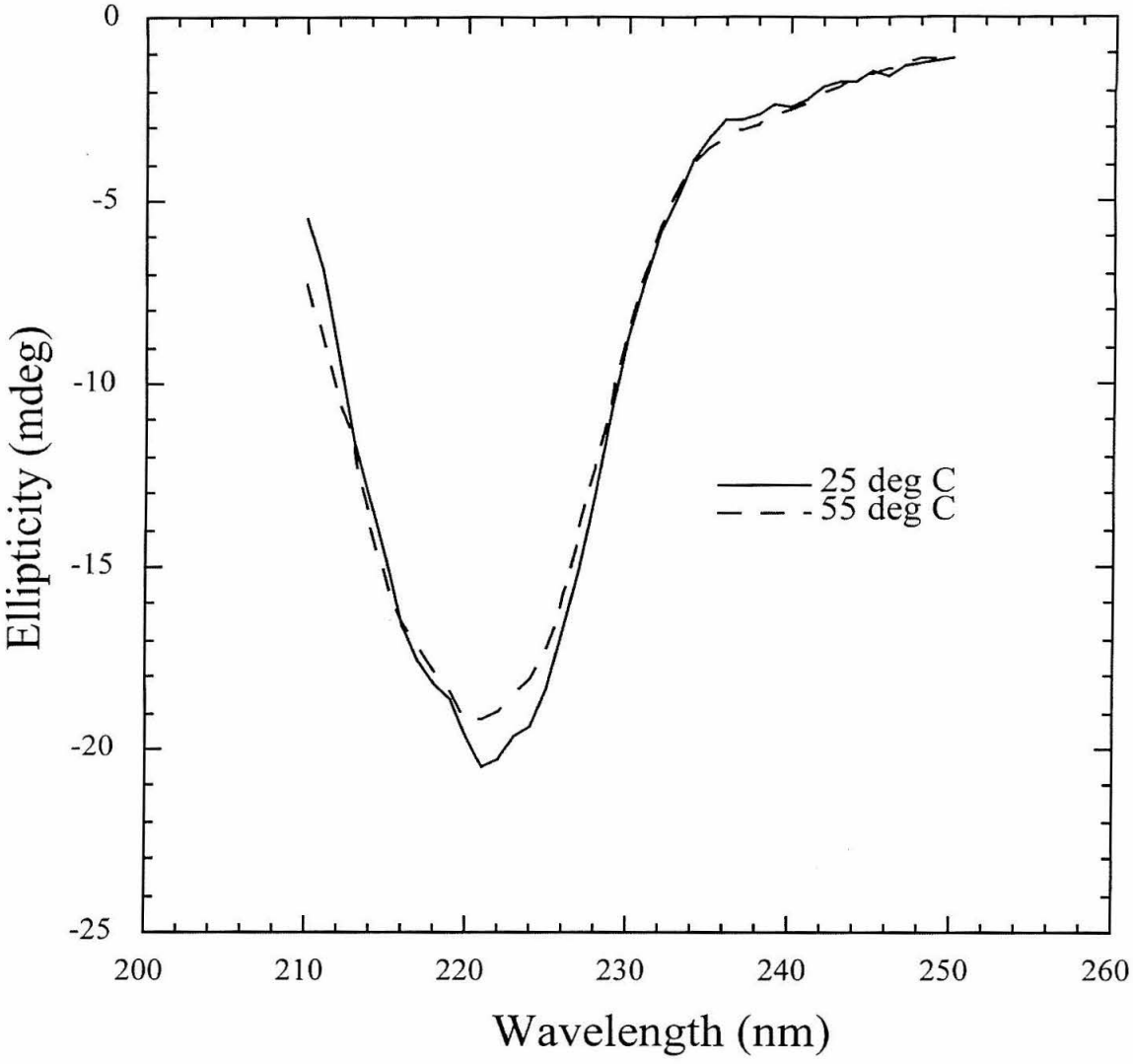
0
-5
-10
-15
-20
-25
Ellipticity (mdeg)
200
210
220
230
240
250
260
Wavelength (nm)
25 deg C
55 deg C

Figure 3.8: Melting curves of reduced wild type amicyanin at pH 8.0 and pH 6.0. The forward melt, taken while increasing the temperature, is represented by a solid line; the reverse melt, taken while decreasing the temperature, is represented by a dashed line. Temperature only raised until the plateau of the I state. Inset: Full CD curves taken before and after the melt/reverse melt process at 25 degrees C. Protein at the beginning of the experiment is represented by the solid curves, while protein after the experiment is represented by the dashed curves. Results indicate the process is reversible at pH 8.0, but irreversible at pH 6.0.

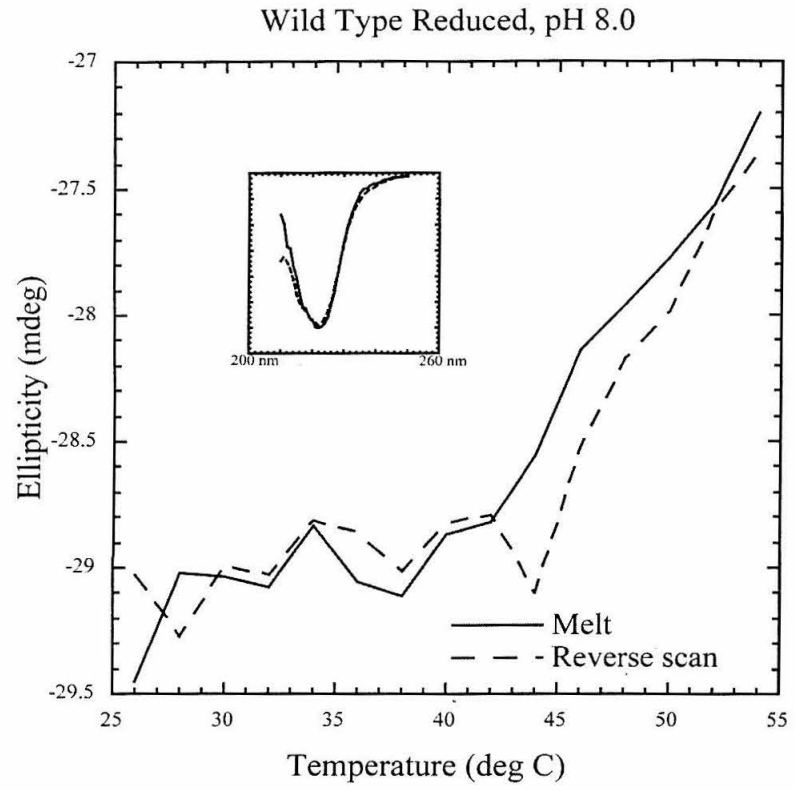
Wild Type Reduced, pH 8.0
Ellipticity (mdeg)
-27
-27.5
-28
-28.5
-29
-29.5
200 nm
260 nm
Melt
Reverse scan
25
30
35
40
45
50
55
Temperature (deg C)

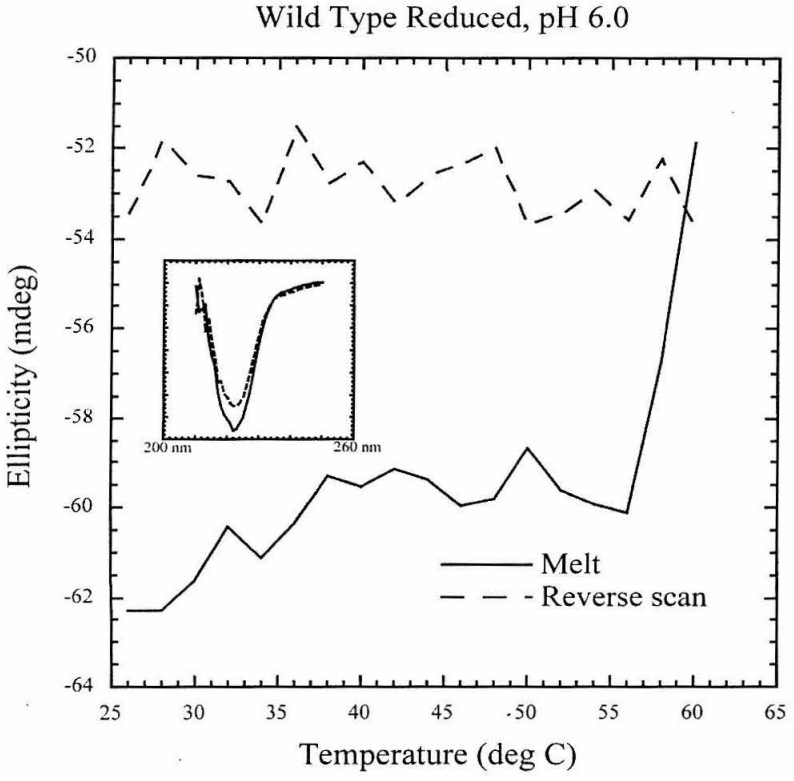
Wild Type Reduced, pH 6.0
Ellipticity (mdeg)
-50
-52
-54
-56
-58
-60
-62
-64
200 nm
260 nm
Melt
Reverse scan
25
30
35
40
45
50
55
60
65
Temperature (deg C)

Figure 3.9: Melting curves of oxidized wild type amicyanin at pH 8.0 and pH 6.0. The forward melt, taken while increasing the temperature, is represented by a solid line; the reverse melt, taken while decreasing the temperature, is represented by a dashed line. Temperature only raised until the plateau of the I state. Inset: Full CD curves taken before and after the melt/reverse melt process at 25 degrees C. Protein at the beginning of the experiment is represented by the solid curves, while protein after the experiment is represented by the dashed curves. Results indicate the process is reversible at pH 8.0, but irreversible at pH 6.0.

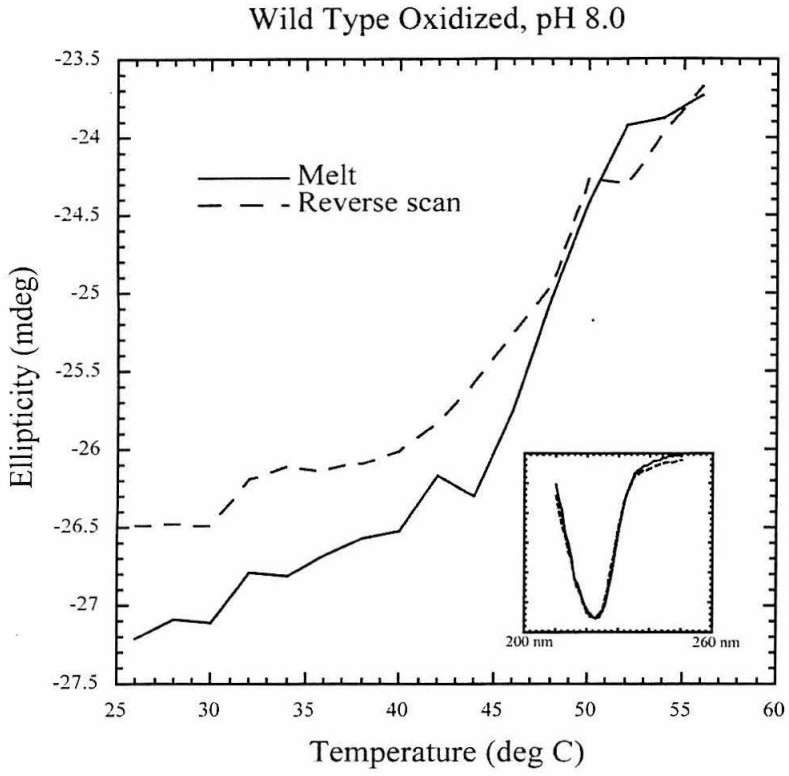
Wild Type Oxidized, pH 8.0
Melt
Reverse scan
Ellipticity (mdeg)
Temperature (deg C)
200 nm
260 nm

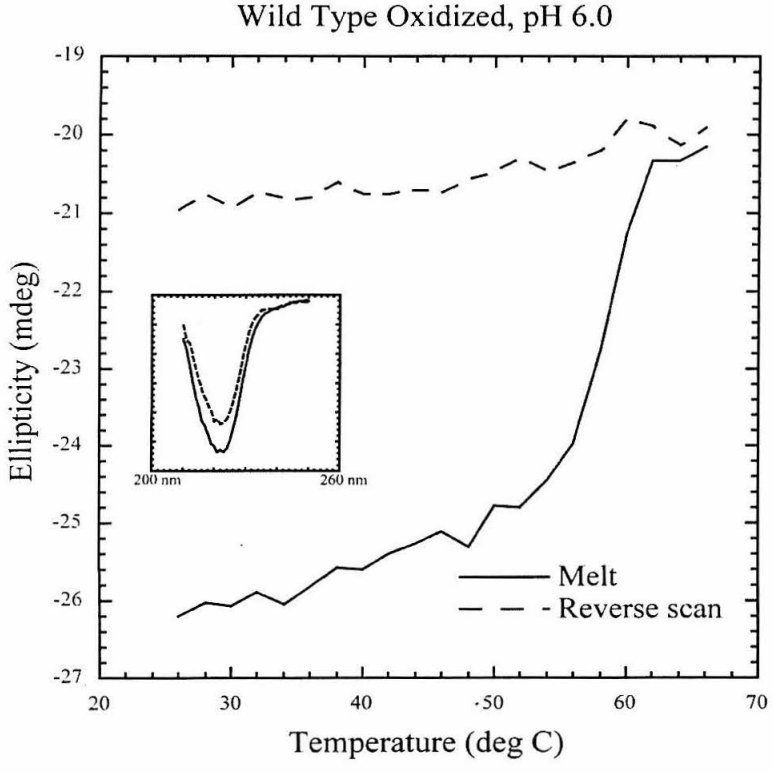
Wild Type Oxidized, pH 6.0
Melt
Reverse scan
Ellipticity (mdeg)
Temperature (deg C)
200 nm
260 nm

Figure 3.10: Melting curves of reduced P94F amicyanin at pH 8.0 and pH 6.0. The forward melt, taken while increasing the temperature, is represented by a solid line; the reverse melt, taken while decreasing the temperature, is represented by a dashed line. Temperature only raised until the plateau of the I state. Inset: Full CD curves taken before and after the melt/reverse melt process at 25 degrees C. Protein at the beginning of the experiment is represented by the solid curves, while protein after the experiment is represented by the dashed curves. Results indicate the process is irreversible at pH 8.0 at both pHs.

P94F Reduced, pH 8.0

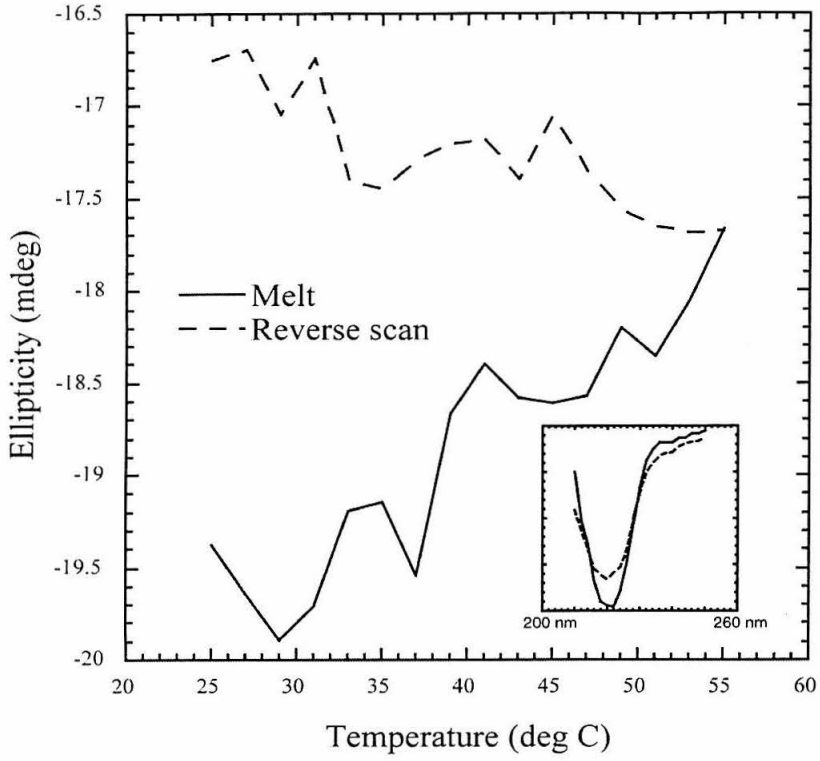

P94F Reduced, pH 8.0

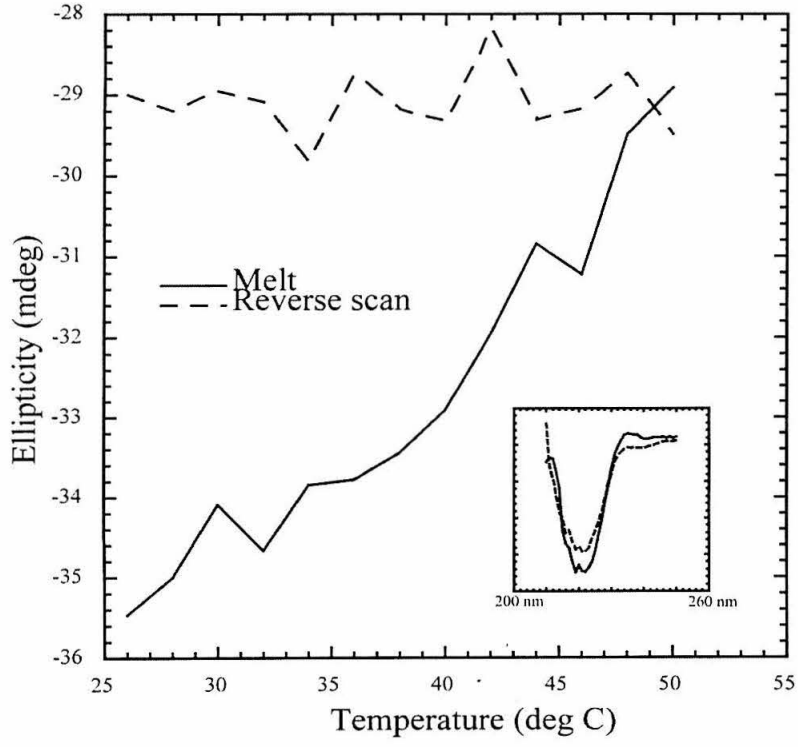

Figure 3.11: EPR spectra of oxidized wild type amicyanin, taken at 77K. I state sample was flash frozen from 328 K. Native was flash frozen from 298 K. Spectra appear identical, indicating that the copper structure of the I state is the same as the structure of the native.

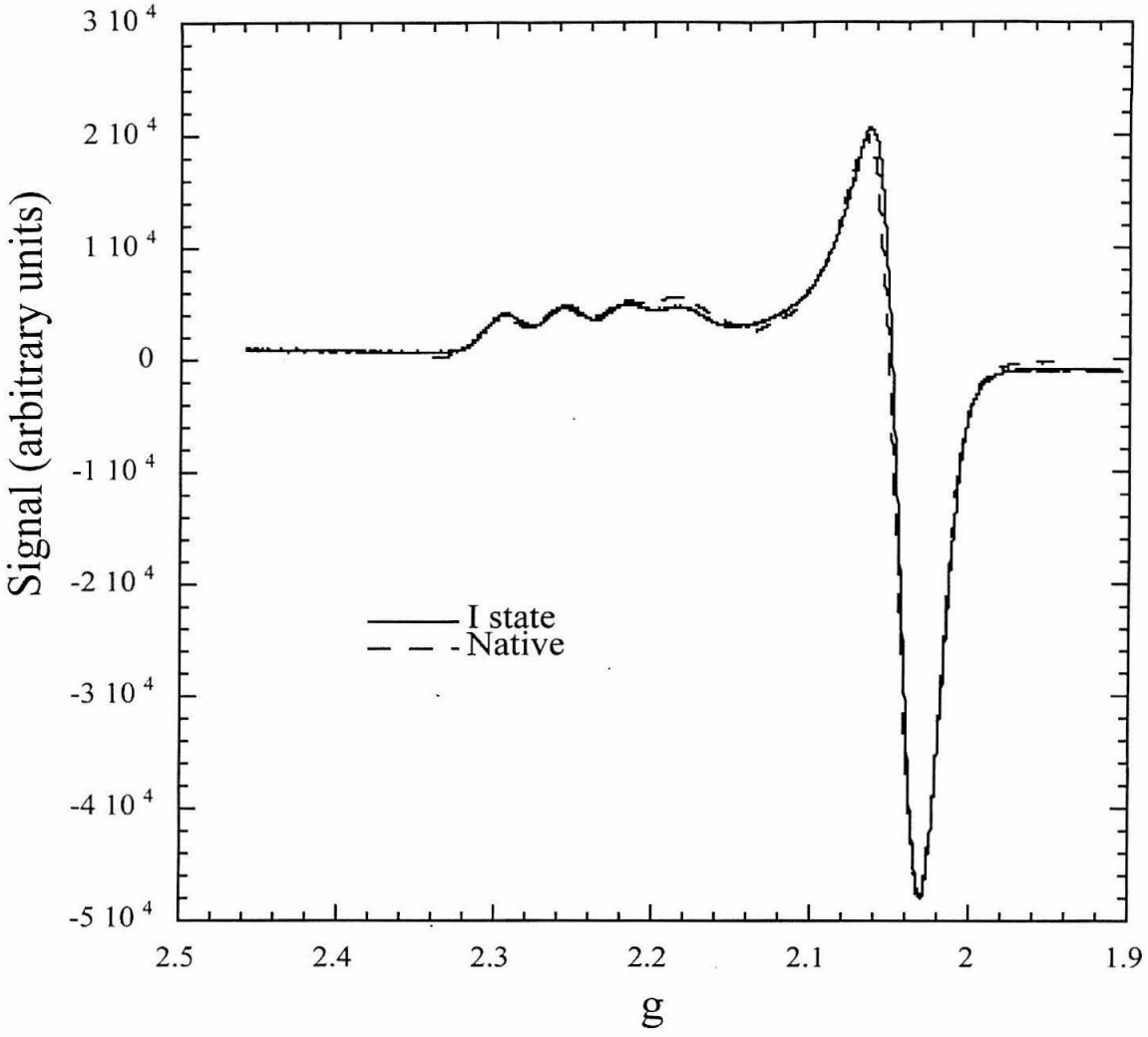
3 10 4
2 10 4
1 10 4
0
-1 10 4
-2 10 4
-3 10 4
-4 10 4
-5 10 4
Signal (arbitrary units)
I state
Native
2.5
2.4
2.3
2.2
2.1
2
1.9
g

Figure 3.12: Plot of E^0/T vs. 1/T: the temperature dependence of the reduction potential of wild type amicyanin.

Temperature Dependence of Wild Type Reduction Potential

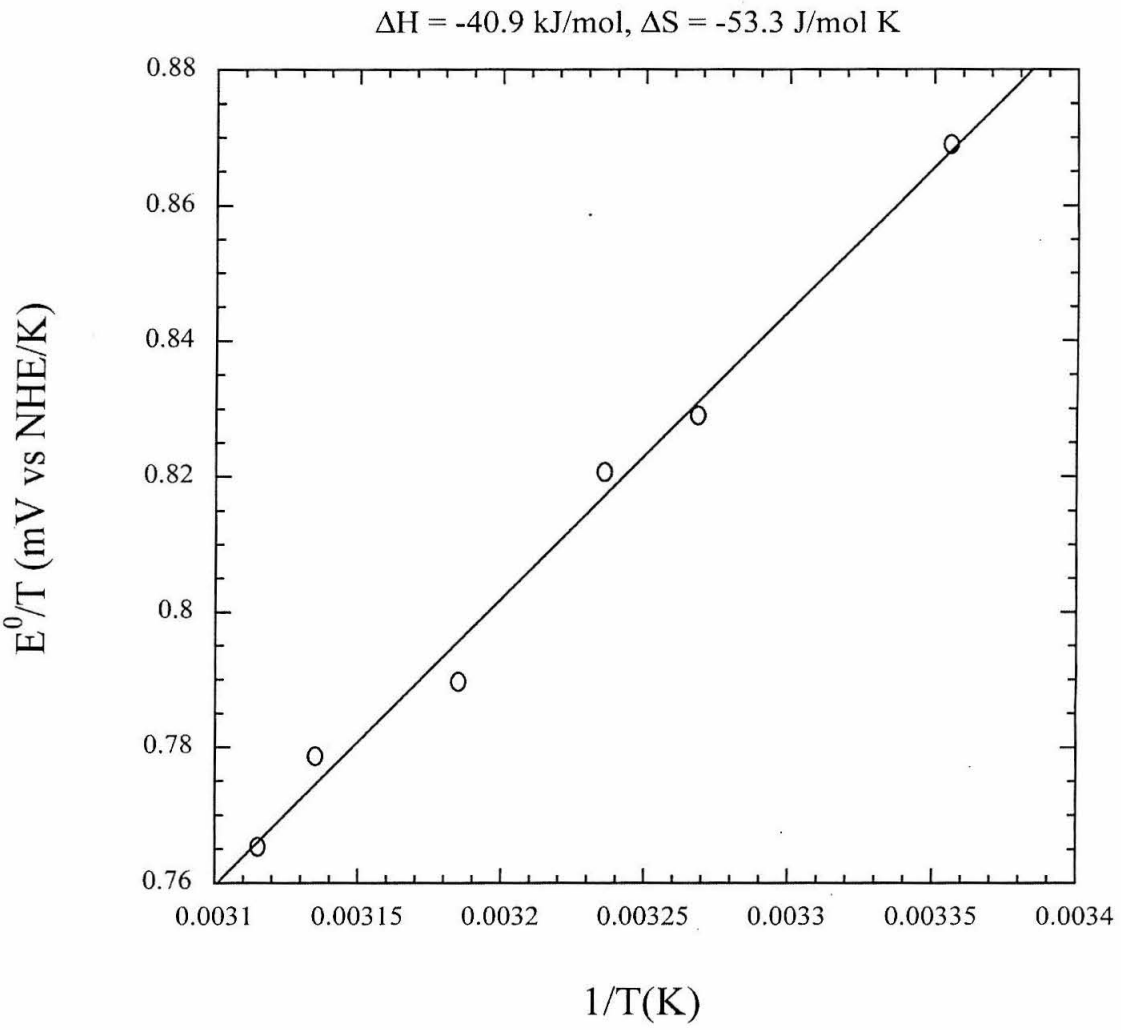

Figure 3.13: Plot of E^0/T vs. 1/T: the temperature dependence of the reduction potential of P94F amicyanin.

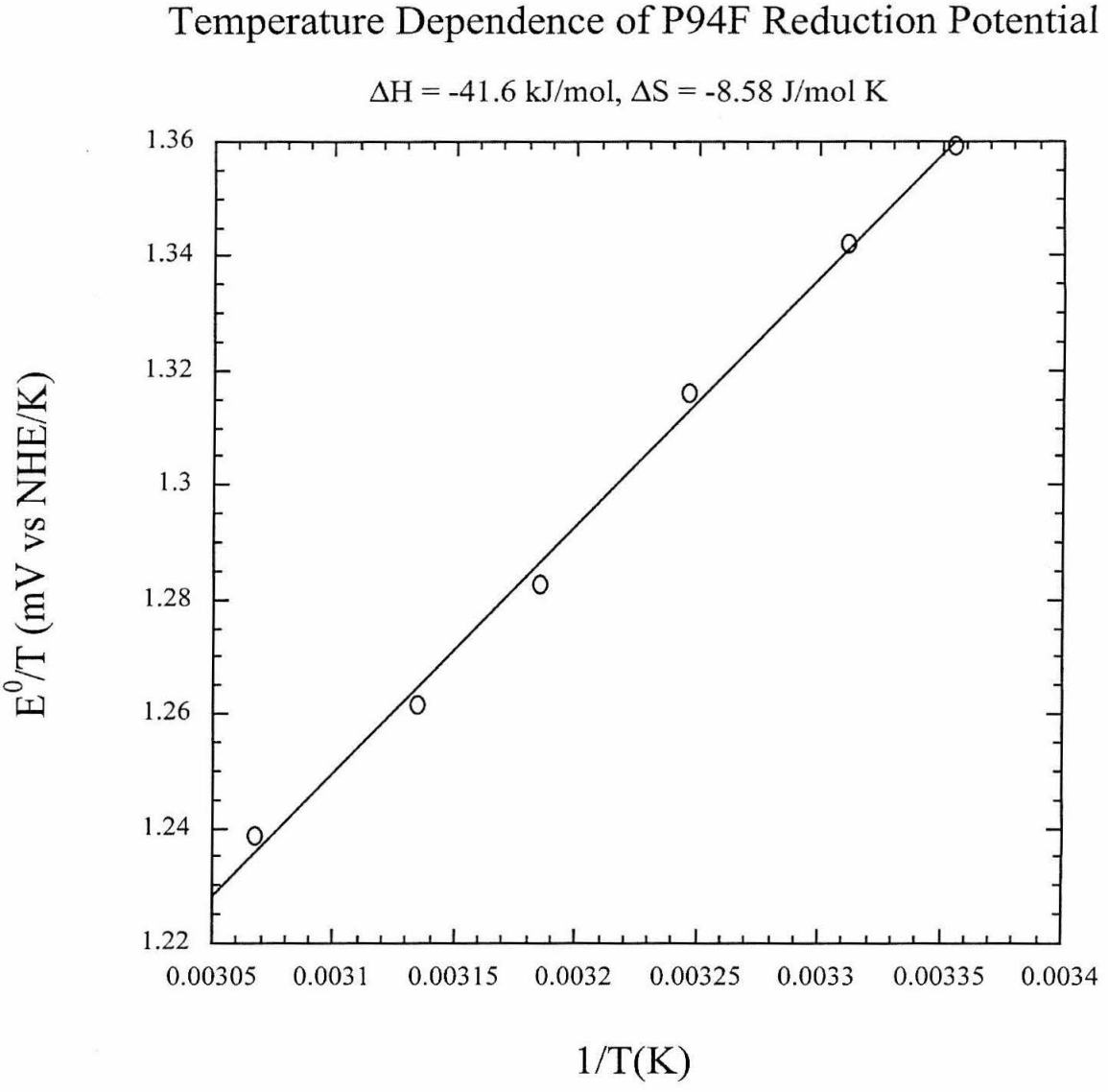
Temperature Dependence of P94F Reduction Potential
ΔH = -41.6 kJ/mol, ΔS = -8.58 J/mol K
E⁰/T (mV vs NHE/K)
1.36
1.34
1.32
1.3
1.28
1.26
1.24
1.22
0.00305
0.0031
0.00315
0.0032
0.00325
0.0033
0.00335
0.0034
1/T(K)

1)Privalov, P. L.; Khechinashvili, N. N. *J. Mol. Biol.* **1974**, *86*, 665-684.

2)Manning, M. C.; Woody, R. W. *Biophys J.* **1986**, *49*, 296a.

3)Luo, J.; California Institute of Technology: Pasadena, CA, 1997, pp 67-110.

4)Coleman, J. E.; Chlebowski, J. F. *Adv. Inorg. Biochem.* **1979**, *1*, 1-67.

5)Muller, N. *Biopolymers* **1993**, *33*, 1185-1193.

6)Privalov, P. L. *Adv. Prot. Chem.* **1979**, *33*.

7)Engeseth, H. R.; McMillin, D. R. *Biochemistry* **1986**, *25*, 2448-2455.

8)Merchant, S.; Bogorad, L. *J. Biol. Chem.* **1986**, *261*, 15850-15853.

9)Koide, S.; Dyson, H. J.; Wright, P. E. *Biochemistry* **1993**, *32*, 12299-12310.

10)Draheim, J. E.; Anderson, G. P.; Duane, J. W.; Gross, E. L. *Biophys. J.* **1986**, *49*, 891-900.

11)Solomon, E. I.; Baldwin, M. J.; Lowery, M. D. *Chem. Rev.* **1992**, *92*, 521-542.

12)Wittung-Stafshede, P.; Gomez, E.; Öhman, A.; Aasa, R.; Villahermosa, R. M.; Leckner, J.; Karlsson, B. G.; Sanders, D.; Fee, J. A.; Winkler, J. R.; Malmström, B. G.; Gray, H. B.; Hill, M. G. *Biochem. Biophys. Acta* **1998**, *1388*, 437-443.

13)Battistuzzi, G.; Borsari, M.; Loschi, L.; Righi, F.; Sola, M. *J. Am. Chem. Soc.* **1999**, *121*, 501-506.

14)Ainscough, E. W.; Bingham, A. G.; Brodie, A. M.; Ellis, W. R.; Gray, H. B.; Loehr, T. M.; Plowman, J. E.; Norris, G. E.; Baker, E. N. *Biochemistry* **1987**, *26*, 71-82.

15)de Pélichy, L. D. G.; Smith, E. T. *Biochemistry* **1999**, *38*, 7874-7880.

16)Guss, J. M.; Merritt, E. A.; Phizackerley, R. P.; Freeman, H. C. *J. Mol. Biol.* **1996**, *262*, 686-705.

17)Hart, P. J.; Nersissian, A. M.; Herrmann, R. G.; Nalbandyan, R. M.; Valentine, J. S.; Eisenberg, D. *Prot. Sci.* **1996**, *5*, 2175-2183.

18)Nar, H.; Messerschmidt, A.; Huber, R.; van de Kamp, M.; Canters, G. W. *J. Mol. Biol.* **1991**, *221*, 765-772.

19)Baker, E. N. *J. Mol. Biol.* **1988**, *203*, 1071-1095.

20)Dunitz, J. D. *Science* **1994**, *24*, 670-670.

21)Taneva, S. G.; Kaiser, U.; Donchev, A. A.; Dimitrov, M. I.; Mäntele, W.; Muga, A. *Biochemistry* **1999**, *38*, 9640-9647.